Measuring dark matter spikes around primordial black holes with Einstein Telescope and Cosmic Explorer

Philippa S. Cole,[1,*] Adam Coogan,[2,3,4,1,†] Bradley J. Kavanagh,[5,‡] and Gianfranco Bertone[1,§]

[1]*Gravitation Astroparticle Physics Amsterdam (GRAPPA), Institute for Theoretical Physics Amsterdam and Delta Institute for Theoretical Physics, University of Amsterdam, Science Park 904, 1098 XH Amsterdam, Netherlands*

[2]*Ciela—Computation and Astrophysical Data Analysis Institute, Montréal, Quebec, Canada*

[3]*Département de Physique, Université de Montréal, 1375 Avenue Thérèse-Lavoie-Roux, Montréal, Quebec H2V 0B3, Canada*

[4]*Mila—Quebec AI Institute, 6666 St-Urbain, #200, Montreal, Quebec H2S 3H1, Canada*

[5]*Instituto de Física de Cantabria (IFCA, UC-CSIC), Avenida de Los Castros s/n, 39005 Santander, Spain*

(Received 2 September 2022; accepted 13 February 2023; published 4 April 2023)

Future ground-based gravitational wave observatories will be ideal probes of the environments surrounding black holes with masses $1-10M_\odot$. Binary black hole mergers with mass ratios of order $q = m_2/m_1 \lesssim 10^{-3}$ can remain in the frequency band of such detectors for months or years, enabling precision searches for modifications of their gravitational waveforms with respect to vacuum inspirals. As a concrete example of an environmental effect, we consider here a population of binary primordial black holes which are expected to be embedded in dense cold dark matter spikes. We provide a viable formation scenario for these systems compatible with all observational constraints and predict upper and lower limits on the merger rates of small-mass-ratio pairs. Given a detected signal of one such system by either Einstein Telescope or Cosmic Explorer, we show that the properties of the binary and of the dark matter spike can be measured to excellent precision with one week's worth of data, if the effect of the dark matter spike on the waveform is taken into account. However, we show that there is a risk of biased parameter inference or missing the events entirely if the effect of the predicted dark matter overdensity around these objects is not properly accounted for.

DOI: 10.1103/PhysRevD.107.083006

I. INTRODUCTION

Future ground-based gravitational wave observatories will be capable of detecting binary black hole mergers at unprecedented distances [1]. While event rates will be dominated by close-to-equal mass mergers, the enhanced sensitivity and wider frequency range of the proposed Einstein Telescope (ET) [2,3] and Cosmic Explorer (CE) [4] observatories will also open the door to observing intermediate-mass-ratio mergers.

The planned frequency ranges of Cosmic Explorer, $f \sim [5, 5000]$ Hz, and Einstein Telescope, $f \sim [1, 5000]$ Hz, mean that the observatories will be sensitive to long duration signals from light systems with mass ratios of order $q = m_2/m_1 \sim 10^{-3}$, where m_1 is the mass of the central compact object and m_2 is the mass of its lighter companion. Binaries with $m_1 = 1$–$10M_\odot$ will remain in band for many months or years. Detecting such systems would have exciting consequences for gravitational wave astronomy as well as fundamental physics [5,6].

Systems with small mass ratios are particularly interesting because they are more likely to be influenced by environmental effects. The gravitational waveform of a binary inspiralling through an environment will be different to that of the equivalent system merging in vacuum. In the case of an environment of collisionless matter, dynamical friction, accretion, and a varying mass enclosed within the orbit alter the dynamics of the binary [7–16]. This appears as a gradual change in the cumulative phase of the waveform with respect to the system in vacuum, detectable if a very large number of cycles are observed. Dense environments are more likely to survive around small-mass-ratio systems, unlike in equal-mass binaries, where any environments are likely to be disrupted on a timescale of a few orbits [17,18]. Given the amount of time these systems will spend in band, this places Einstein Telescope and Cosmic Explorer well to detect this *dephasing* effect in small-mass-ratio binaries.

In this work, we explore how well ET and CE can measure the properties of primordial black hole (PBH)

*p.s.cole@uva.nl
†adam.coogan@umontreal.ca
‡kavanagh@ifca.unican.es
§g.bertone@uva.nl

binaries embedded in cold dark matter (DM) spikes. PBHs may be formed shortly after the end of inflation from large density fluctuations, contributing to the nonbaryonic content of the Universe [19]. However, PBHs cannot make up all of the dark matter by themselves in the stellar mass range (see e.g. [20,21] for caveats) and therefore must be accompanied by another dark component. If the remaining DM is made up of cold, collisionless particles, it will form dense spikes around primordial black holes with a well-defined density profile [22–25], which will have an effect on a PBH binary's dynamics. Intermediate- or extreme-mass-ratio PBH binaries can therefore only be found and correctly interpreted if the effect of the dark matter spike is taken into account. Moreover, electromagnetic signatures of DM spikes around PBHs are largely ruled out for $f_{\rm PBH} \gtrsim 10^{-8}$ [26–29], making gravitational wave searches a particularly promising avenue for discovery of such mixed DM scenarios.

We show that Einstein Telescope and Cosmic Explorer are ideally positioned to observe gravitational wave signals from dark matter-dressed PBH binaries. In particular, the range of gravitational wave (GW) frequencies accessible to both experiments makes them sensitive to solar and subsolar mass PBH binaries in the local Universe (Sec. II). We provide a concrete formation scenario for such PBH binaries and predict upper and lower limits on the merger rates of intermediate-mass-ratio pairs (Sec. III). We specify the properties of the DM spikes which are expected to form around PBHs and describe how the influence of these DM spikes on the gravitational waveform can be modeled (Sec. IV). With these tools, we show that it will be possible to distinguish these systems from GR-in-vacuum inspirals and to measure the properties of the binary and the dark matter spike (Secs. V and VI). This is only possible if parameter estimation is conducted with waveform templates that take into account the effects of dynamical friction; we risk missing these signals in the data if it is assumed that all binaries are inspiralling in vacuum. We conclude by discussing these challenges associated with realistic search and inference strategies, as well as relevance of our results to other environmental effects around BH binaries (Sec. VII).

II. EINSTEIN TELESCOPE AND COSMIC EXPLORER REACH

Firstly, we assess which systems are best placed to be detected by various observatories.

The improvement in sensitivity and frequency reach of Einstein Telescope and Cosmic Explorer beyond aLIGO is shown by the noise power spectral density curves $S_n(t)$ in Fig. 1.[1] Throughout this paper, we choose our "benchmark" PBH binary to have masses $m_1 = 1M_\odot$ and $m_2 = 10^{-3}M_\odot$. The characteristic strain [31] of the gravitational wave signal caused by the inspiralling of black holes with these masses is shown by the rightmost black line in Fig. 1, for one week's worth of frequency evolution. This system lies very nicely in the frequency range of the future ground-based detectors. The presence of a dense DM spike around the heavier PBH will influence the precise frequency evolution of the system, while the inspiral of the binary will lead to a gradual depletion of the spike due to feedback effects [15].

The black dot on each trajectory in Fig. 1 marks the "break frequency" f_b; at frequencies below f_b the timescale for the depletion of the DM spike is much shorter than the timescale for inspiral due to GW emission, while at frequencies above f_b the evolution of the DM spike becomes negligible. This parametrization in terms of f_b is relevant for calculating the effects of feedback on the spike and will be discussed later in Sec. IV. As argued in Ref. [16], the important point is that in order to detect the dephasing of the gravitational waveform, the break frequency should lie in a region of high sensitivity of the detector. In addition, the system should remain in band for a long time period so that as many dephased cycles as possible are observed. For example, for this benchmark system with a year of observations, approximately 10^7 cycles occur in band.

For comparison, we also show the Laser Interferometer Space Antenna (LISA) noise curve which lies at far lower frequencies, making it more suited to observing the higher-mass systems which have previously been studied in the context of DM-induced dephasing [7,8,12–16,32–36]. We also plot the characteristic strain for five years worth of frequency evolution of the system with $m_1 = 10^3 M_\odot$ and $m_2 = 1.4M_\odot$ embedded in a dark matter spike, which was explored in Ref. [16]. It was shown that the properties of the dark matter spike could be reconstructed to very good accuracy with five years of observations and motivates this investigation into what future ground-based observatories can do for dark matter spike searches.

For each detector, the distance at which our benchmark system will be detectable varies. We calculate the SNR averaged over sky position, orientation and polarization angle as a function of chirp mass $\mathcal{M} = (m_1 m_2)^{\frac{3}{5}}/(m_1 + m_2)^{\frac{1}{5}}$ and luminosity distance to source d_L via

$$\mathrm{SNR} = \frac{1}{d_L}\sqrt{4\int \frac{4}{5}\frac{h_0^2(f)}{S_n(f)}\mathrm{d}f}, \tag{1}$$

where $S_n(f)$ is the power spectral density for a detector and the amplitude of the Fourier transform of the gravitational waveform h_0 is constructed from the following expressions for the phase Φ and its derivatives with respect to time [37]:

[1]Note that Einstein Telescope is configured as an equilateral triangle with an interferometer at each vertex. To account for this, we shift the noise power spectral density down by 18% [30].

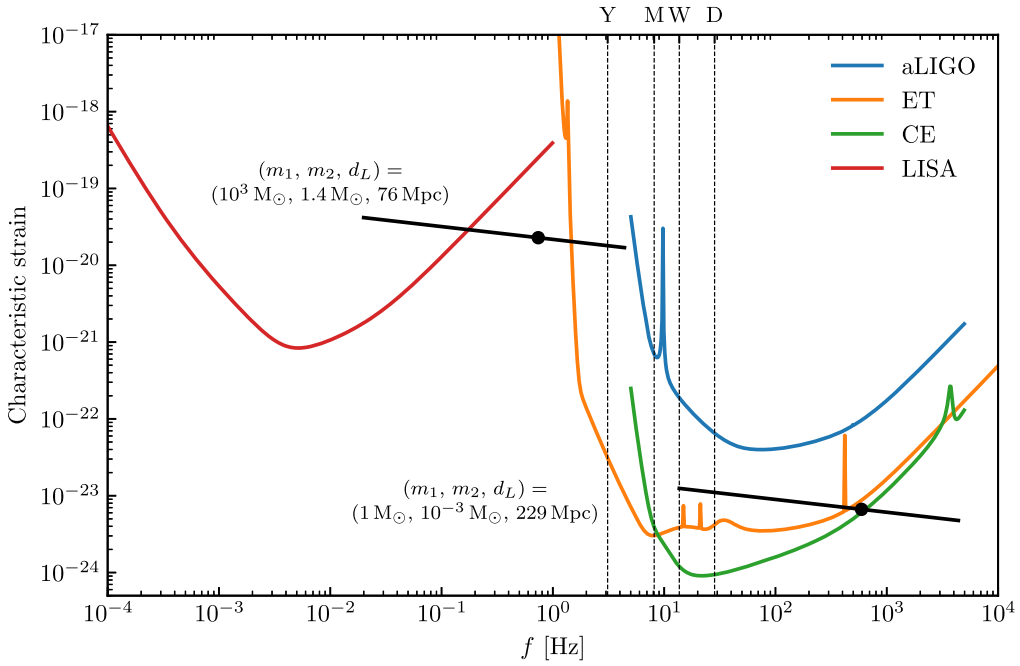

FIG. 1. Characteristic strain as a function of frequency for the noise in various detectors as well as two primordial dark dress systems. The heavy and light systems "trajectories" (thick black lines) begin five years and one week before the innermost stable circular orbit frequency. The systems' distances were, respectively, chosen to given signal-to-noise ratios of 15 at LISA and 12 at Cosmic Explorer over these observing durations. The vertical dashed lines indicate the frequencies at a year, month, week and day before coalescence for the light binary. The black dots indicate the frequency above which depletion of the spike via dynamical friction from the compact object becomes negligible (see Sec. IV). The system in the LISA band was studied in detail in Ref. [16].

$$
\begin{aligned}
h_0(f) &= \frac{1}{2}\frac{4\pi^{2/3}G^{5/3}\mathcal{M}^{5/3}f^{2/3}}{c^4}\sqrt{\frac{2\pi}{\ddot{\Phi}}},\\
\ddot{\Phi} &= 4\pi^2 f\left(\frac{\mathrm{d}\Phi}{\mathrm{d}f}\right)^{-1},\\
\Phi(f) &= \int_f^{f_{\mathrm{ISCO}}}\frac{\mathrm{d}t}{\mathrm{d}f'}f'\mathrm{d}f',\\
t(f) &= \frac{1}{2\pi}\int^f\frac{\mathrm{d}f'}{f'}\frac{\mathrm{d}\Phi}{\mathrm{d}f}.
\end{aligned}
\tag{2}
$$

Here G is Newton's gravitational constant, c is the speed of light, and f_{ISCO} is the GW frequency at the innermost stable circular orbit (ISCO), which we take to be the point of merger.

The SNRs for aLIGO, ET and CE are shown in Fig. 2 where we highlight an SNR threshold of 12 as our definition of detectability, although note that this threshold could be lowered if multiple detectors are online simultaneously. With aLIGO, our benchmark system would only be detectable within a small volume of < 300 Mpc^3. However, for ET this increases to 10^6 Mpc^3 and for CE to $\sim 3 \times 10^7$ Mpc^3.

We will now estimate the merger rates that we can expect for these light systems and use the distances calculated above for an SNR threshold of 12 to predict the number of events we can hope to detect per year.

III. PBH MERGER RATE

We now calculate how many PBH mergers with small mass ratios $q < 10^{-2.5}$ we can hope to detect with ET and CE. We first calculate the distribution of PBHs that can be expected to form from a primordial power spectrum which is boosted by 6–7 orders of magnitude with respect to the observed amplitude on cosmic microwave background (CMB) scales. We then calculate the merger rate for this population and isolate those with mass ratios where a dark matter spike is expected to have survived around the larger of the two black holes.

We do not account for the effect of the DM spikes on the PBH merger rate, as was done in for example Ref. [15] for equal-mass mergers. In principle, dynamical friction from the DM spike may reduce the merger time of the binary, affecting the predicted merger rate for these systems. However, detailed calculations have not yet been performed for the intermediate- and extreme-mass-ratio PBH binaries we consider here (though see Ref. [38] for recent work on circumbinary accretion of DM). We also neglect the effects of baryonic accretion on the PBH merger rate, which is relevant only for PBH masses larger than a few solar masses [39].

A. PBH mass function

As a concrete example of a realization of PBH formation, we assume that PBHs can form from large overdensities

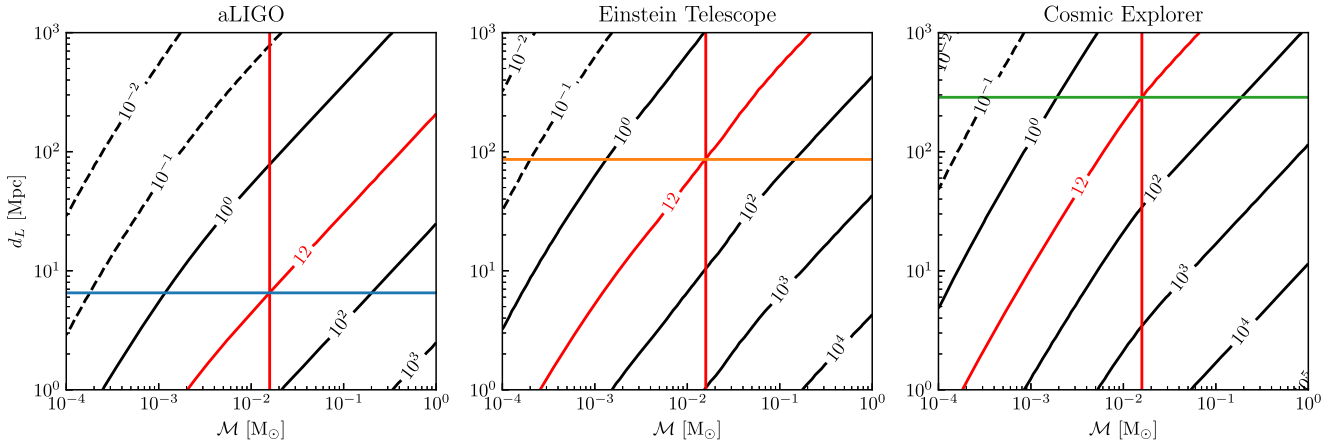

FIG. 2. SNRs for benchmark system observed by terrestrial detectors. The vertical red line indicates the chirp mass of our benchmark $(m_1, m_2) = (1, 10^{-3})M_\odot$ system. The horizontal lines indicate the distances at which this system would have an (optimal) SNR of 12 in each detector, with their colors matching the ones used in Fig. 1. The diagonal contours indicate curves of constant SNR, with the red one highlighting the special value of 12 which we use to define a system as detectable. Note that the SNR for vacuum binaries and the dark dresses we consider is the same since it is not substantially altered by the DM spike. Since a vacuum binary's frequency at merger is not purely a function of its chirp mass, in this plot we assume each system is observed for 1 week up to the high-frequency cutoff for each detector.

which collapse shortly after single-field inflation. We assume an initially Gaussian density field and that there is no clustering; however see [21,40–44] for other possibilities. Note that PBHs can also form from e.g. the collapse of cosmic strings [45,46] or during phase transitions in the early Universe [47–49].

A reference primordial power spectrum (PPS) that satisfies all current constraints can be modeled by a piecewise power law spectrum [50,51]:

$$\mathcal{P}_\mathcal{R}(k) = A \begin{cases} (\frac{k}{k_p})^{n_g} & k \leq k_p, \\ (\frac{k}{k_p})^{-n_d} & k > k_p. \end{cases} \tag{3}$$

We choose $n_g = 4$ because it is representative of peaks produced via ultra-slow-roll models of inflation [50,51], and we choose $n_d = 0.05$ as being the slowest decay possible (in order to enhance production of light PBHs) without conflicting with observational constraints on scales smaller than the peak [52]. We then compute the mass function of PBHs that would be formed, shown in Fig. 3, using the Press-Schechter formalism as laid out in Ref. [52] and accounting for the effect of the evolving equation of state in the early Universe [53,54]. This results in a mass function with multiple peaks owing to the fact that PBHs form more easily at times when the equation of state was lower. The most prominent peak is around $1M_\odot$, because scales with this horizon mass were collapsing at the time of the QCD phase transition, where the equation of state decreases by a factor of $\sim 1/3$ [54]. Since we are interested in stellar-mass black holes, we choose $k_p = 10^6$ Mpc^{-1} such that solar-mass PBHs are preferentially produced and this further motivates our choice of benchmark mass $m_1 = 1M_\odot$.

We do not take into account various considerations that may affect the relationship between the amplitude of the primordial power spectrum and the PBH abundance [55], for example non-Gaussianity, the shape of the curvature perturbation [56] or the nonlinear relationship between the density and curvature perturbation [57–59] because we are not trying to constrain $f_{\rm PBH}$ with a specific amplitude of the power spectrum. Instead, we fix the shape of the spectrum and then have the freedom to vary A in order to obey $f_{\rm PBH}$ constraints or to absorb subtleties in the calculation of $f_{\rm PBH}$ from the initial distribution of densities. We note that if the initial conditions are non-Gaussian, the initial distribution of PBHs will be clustered, and this will effect the

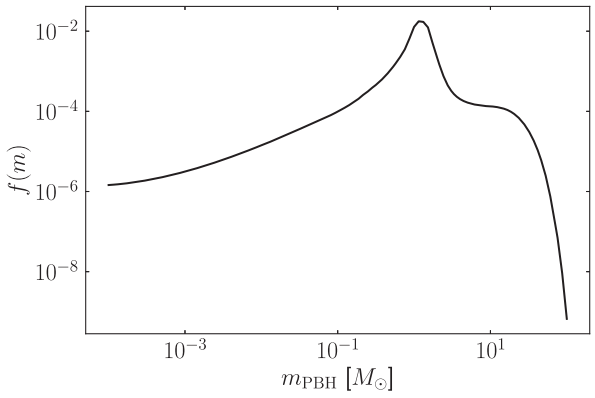

FIG. 3. The mass function of PBHs adopted in this work. We normalize the mass function according to $\int f(m) \mathrm{d} \ln m = f_{\rm PBH}$. The multiple peak structure arises from the evolving equation of state in the early Universe [53]. The peak of the primordial power spectrum is at $k_p = 10^6$ Mpc^{-1}, and the abundance of PBHs in this case is $f_{\rm PBH} = 0.013$.

merger rate. However, it is uncertain how much the merger rate is affected as the level of non-Gaussianity increases [42,60], and such initial clustering from non-Gaussianities may be constrained by measurements of CMB μ distortions [61,62].

We find that, for $k_p = 10^6$ Mpc^{-1}, an amplitude of $A = 3 \times 10^{-3}$ saturates the constraints as described below in Sec. III C and leads to $f_{\rm PBH} = 0.013$.

B. Differential merger rate calculation

Two neighboring PBHs may form a binary in the early Universe when their self-gravity dominates over the Hubble flow [63–65]. Two further requirements are that the radial tidal forces from all other PBHs and matter fluctuations are weaker than the attraction of the pair and that the tidal torques large enough to prevent a head-on collision [66,67].

The differential merger rate for PBH binaries formed in the early Universe [early-forming binaries (EB) being dominant over those formed by tidal capture in PBH clusters in the late Universe [68–70], at least for small values of $f_{\rm PBH}$] with component masses m_1 and m_2 is given by [71–73]

$$\mathrm{d}R_{\rm EB} = f_{\rm SUP}\frac{1.6\times10^6}{\mathrm{Gpc^3\,yr}} f_{\rm PBH}^{\frac{53}{37}}\eta^{-\frac{34}{37}}\left(\frac{m_1+m_2}{M_\odot}\right)^{-\frac{32}{37}} \times\left(\frac{t}{t_0}\right)^{-\frac{34}{37}}\psi(m_1)\psi(m_2)\mathrm{d}m_1\mathrm{d}m_2, \tag{4}$$

where $f_{\rm SUP}$ is the so-called suppression factor (details below), $\eta = m_1m_2/(m_1+m_2)^2$, t is the cosmic time of merger, t_0 is the cosmic time today, and $\psi(m)$ is the mass function defined by

$$\int m\psi(m)\mathrm{d}\ln m = \int \frac{f(m)}{f_{\rm PBH}}\mathrm{d}\ln m = 1, \tag{5}$$

where the second equality demonstrates the relationship with the notation for the mass function $f(m)$ as plotted in Fig. 3 for clarity. The differential merger rate calculated for the mass function in Fig. 3, including the suppression factor, is shown in Fig. 4.

However, it is very important to note that this merger rate is only reliable for $f_{\rm PBH} \ll 1$, which we satisfy, because otherwise PBH clusters may form that would perturb binaries [74–76]. It is also only valid for relatively narrow mass functions. Since we are using a very broad mass function and are especially reporting merger rates for low mass ratios because those are the binaries where the DM spike will survive, caution must be used. The reason for this is that the suppression factor assumes that a population of lower mass black holes will cause third-body disruption to binaries. However, a large population of very low mass black holes are unlikely to take part in this process very effectively. It is not clear by how much the rate is underestimated, and that study is beyond the scope of this work, so we instead report upper and lower bounds based on using $f_{\rm SUP}$ as in Ref. [73], which approximates the formulations in Refs. [71,72]:

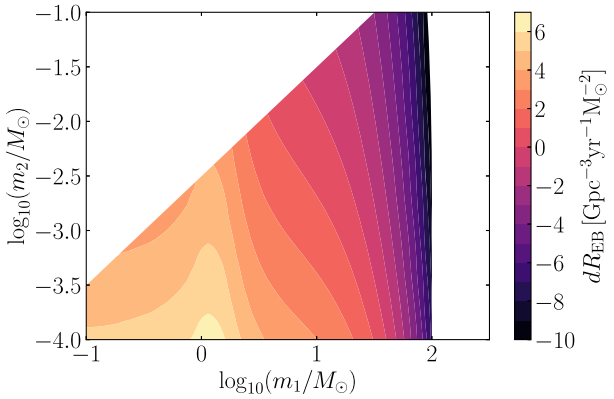

FIG. 4. Differential merger rate of binaries formed in the early Universe, with $m_2 < 10^{-2.5}m_1$, including suppression factor (and therefore an underestimate).

$$f_{\rm SUP} = S_1 \times S_2, \tag{6}$$

with

$$S_1 = 1.42\left(\frac{\langle m_{\rm PBH}^2\rangle/\langle m_{\rm PBH}\rangle^2}{\bar{N}+C} + \frac{\sigma_M^2}{f_{\rm PBH}^2}\right)^{-\frac{21}{74}} e^{-\bar{N}}, \tag{7}$$

$$S_2 \approx \min\left(1, 9.6\times10^{-3} f_{\rm PBH}^{-0.65} e^{0.03\log^2(f_{\rm PBH})}\right), \tag{8}$$

where $\langle m_{\rm PBH}^2\rangle$ and $\langle m_{\rm PBH}\rangle^2$ are the variance and squared mean of the PBH mass, respectively, $\sigma_M^2 = 0.005$, and $\bar{N}$ (for which we use the full expression rather than the upper and lower limits given in Ref. [73]) and C are given, respectively, by

$$\bar{N} = \frac{m_1+m_2}{\langle m_{\rm PBH}\rangle}\frac{f_{\rm PBH}}{f_{\rm PBH}+\sigma_M}, \tag{9}$$

$$C = \frac{f_{\rm PBH}^2\langle m_{\rm PBH}^2\rangle}{\sigma_M^2\langle m_{\rm PBH}\rangle^2}\left[\left(\frac{\Gamma(\frac{29}{37})}{\sqrt{\pi}}U\left(\frac{21}{74},\frac{1}{2},\frac{5f_{\rm PBH}^2}{6\sigma_M^2}\right)\right)^{-\frac{74}{21}} - 1\right]^{-1}, \tag{10}$$

with Γ the gamma function and U the confluent hypergeometric function. The expression for $\bar{N}$ determines the effect of nearby PBHs on the merger rate and using the full expression oversuppresses the merger rate. This gives us our lower bound in all of the merger rate plots, while $f_{\rm SUP} = 1$ (i.e. no effect) gives us our upper bound. Given that we have produced the largest possible merger rate by maximizing the amplitude of the PPS, a detection in the observing runs of ET and CE would put tight constraints on $f_{\rm SUP}$, modulo effects on the merger rate caused by the dark matter spikes. Nondetection would constrain combinations

of $f_{\rm SUP}$ and power spectrum amplitude A but would not break that degeneracy.

C. Saturating observational constraints

In order to determine the most optimistic merger rate in this scenario, we saturate direct constraints on the PBH abundance. We do so by increasing the amplitude of the PPS A until we hit the strongest constraints. At the time of writing, LIGO/Virgo stochastic gravitational wave background (SGWB) spectrum constraints due to binary black hole mergers[2] and the envelope of microlensing constraints from various probes on the subsolar mass range are the strongest on the relevant scales [19,85].

We calculate the resulting stochastic gravitational wave signal due to all mergers by inputting Eq. (4) into the expression from Refs. [71,86,87]:

$$\frac{\mathrm{d}\Omega_{\rm GW}(f)}{\mathrm{d}m_1\mathrm{d}m_2\mathrm{d}z} = \frac{f}{\rho_c c^2 H(z)(1+z)}\frac{\mathrm{d}E_{\rm GW}}{\mathrm{d}f}(f_r) \times \frac{\mathrm{d}R_{\rm EB}(m_1,m_2)}{\mathrm{d}m_1\mathrm{d}m_2}, \tag{11}$$

with $H(z)$ the Hubble factor and ρ_c the critical density. The observed GW frequency f is related to the source-frame frequency as $f_r = (1+z)f$, and the GW spectrum $\mathrm{d}E_{\rm GW}/\mathrm{d}f$ from merging BHs is given in Appendix A.

We then integrate over all m_1 and m_2, dividing by 2 to avoid double counting, and we integrate between $z = 0$ and $z_{\rm eq}$. We increase the amplitude of the primordial power spectrum [which filters through to $f(m)$] until the spectrum without suppression factor hits the LIGO/Virgo O5 sensitivity curve. This means that the merger rates we now report will be viable by the time ET and CE come online in terms of being compatible with other gravitational wave constraints that will be realized in the meantime.

The microlensing constraints do not depend directly on the merger rate, since they search for distinctive variations in stellar light curves due to individual black holes passing in front of stars in the center of the Milky Way or in nearby galaxies [88–91]. Therefore, using our results for the mass function $f(m)$ and the prescription in Ref. [92], we check that the value of $f_{\rm PBH}$ corresponding to $k_{\rm p} = 10^6$ Mpc^{-1} and $A = 3\times10^{-3}$ which saturates the SGWB constraints is below the threshold allowed by the microlensing constraints from Fig. 3 of Ref. [19]. Indeed, $f_{\rm PBH} = 0.013$ while the constraints require $f_{\rm PBH} < 0.78$.

D. Binned merger rates

The merger rates of a central black hole of mass m_1, within a bin of width $\pm0.5M_\odot$, merging with all masses below $10^{-2.5}m_1$ are shown in Fig. 5. All rates are averaged between redshifts 0 and 0.1, and the upper and lower limits of the filled regions are calculated without and with the suppression factor, respectively. The maximum merger rate we find is $R_{\rm EB} \sim 2400$ Gpc^{-3} yr^{-1} for $m_1 = 1M_\odot$ without suppression factor and $R_{\rm EB} \sim 300$ Gpc^{-3} yr^{-1} with the suppression factor which acts as a lower bound.

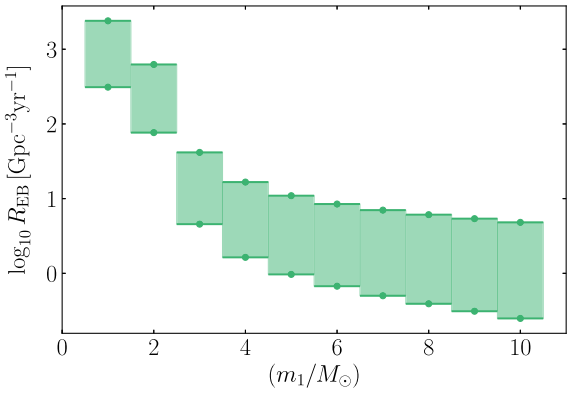

FIG. 5. PBH merger rate for $m_1 \pm 0.5M_\odot$, including mergers with all secondary masses below $m_2 < 10^{-2.5}m_1$. The lower value of the filled region is calculated including the suppression factor of Eq. (6) (and therefore an underestimate), while the upper value is calculated without. All rates are averaged between redshift 0 and 0.1.

In order to report an event rate for a specific benchmark system, we can combine the binned merger rate for $m_1 = 1\pm0.5M_\odot$ and $m_2 = 10^{-3}m_1$, shown in Fig. 6, with the observable volumes of each detector from Sec. II. We find that aLIGO, ET and CE can expect to observe up to 1×10^{-4}, 0.2 and 9 events with an SNR of at least 12 per year, respectively.

Furthermore, we would expect to see larger mass-ratio mergers (where the spike will have been disrupted) occurring in vacuum. For example, for mass ratios of $q = 10^{-1}$

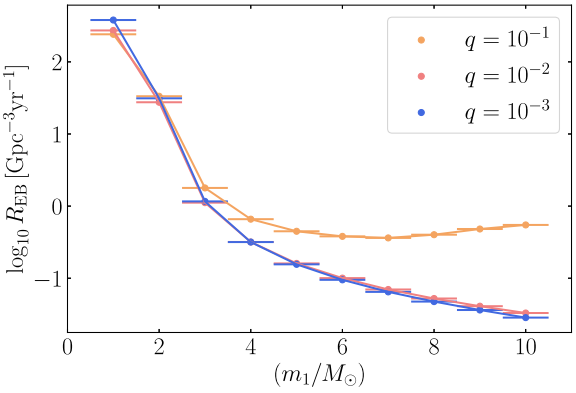

FIG. 6. Merger rate of black hole binaries with $q = 10^{-3}, 10^{-2}, 10^{-1}$, without suppression factor. All averaged between redshift 0 and 0.1. The merger rate for our benchmark system is given by the leftmost bin of the $q = 10^{-3}$ case.

[2]Constraints from the direct observations of individual mergers with LIGO/Virgo/Kagra are typically weaker than those from the SGWB in the subsolar mass range (see e.g. [72,77–84]).

and $q = 10^{-2}$, the expected merger rates for our most optimistic model are also shown in Fig. 6. LIGO/Virgo searches such as Refs. [93,94] can probe these mass ranges but are not sensitive enough to probe these merger rates yet. However, ET and CE will be sensitive enough to search for these vacuum systems [95]. If the merger rate for this region of the parameter space was observed to be in line with the rates presented in Fig. 6, this would be a strong hint that the more extreme-mass-ratio systems, with dark matter spikes, exist.

E. Spike survival

Finally, in order to ensure that the spike will survive the first few encounters of the inspiral, we check that the radius of closest approach is larger than the separation of the binary at the lowest value of the detectors' frequency range, $f_{\rm low}$, for our benchmark masses. The radius of closest approach is

$$r_{\rm min} = a\left(1 - \sqrt{1 - j^2}\right), \tag{12}$$

where a is the semimajor axis of the binary and j is the angular momentum (related to the eccentricity by $j = \sqrt{1 - e^2}$). We fix the time of coalescence of the binary system to be 13 Gyr:

$$t_{\rm coa} = \frac{3a^4 j^7 c^5}{85 m_1 m_2 (m_1 + m_2) G^3} = 13\ {\rm Gyr} \tag{13}$$

and then select the most probable values of a and j that satisfy this using Eq. (5) of Ref. [18] to compare with $r_{\rm low} = (G(m_1 + m_2)/(f_{\rm low}^2 \pi^2))^{\frac{1}{3}}$. We plot the probability distribution in Fig. 7, highlighting $t_{\rm coa} = 13$ Gyr with the green line. For a relevant range of values of a and j, we find $r_{\rm min}/r_{\rm low} > 10$. This means that the first encounter while the orbit is still elliptical should not destroy the spike within the radius that corresponds to the lower end of the frequency band of ET and CE, $f_{\rm low} = 3$ Hz.

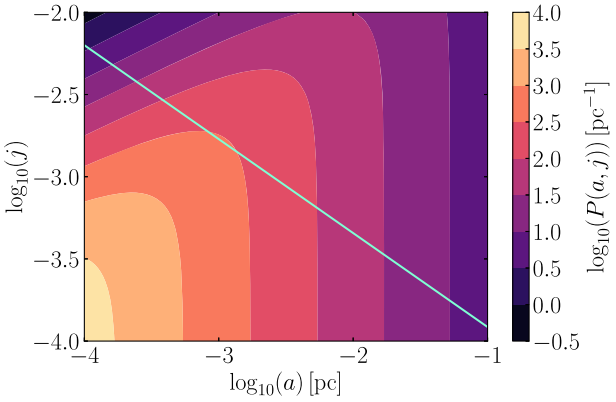

FIG. 7. Probability distribution of PBH binaries that decouple in the early Universe as a function of semimajor axis and angular momentum. The green line represents a coalescence time of 13 Gyr.

Then, using the definition of the tidal radius of the companion object from Eq. (4) of Ref. [96] which is a refinement of the Roche limit that does not treat the central black hole as a point mass, we more stringently check that for a separation given by the radius of closest approach $r_{\rm min}$, the tidal radius is still greater than $r_{\rm low}$. This is indeed the case with $r_{\rm tidal}/r_{\rm low} > 2$ for the most probable range of semimajor axes.

IV. DEPHASING DUE TO DARK MATTER SPIKE

Now that we have seen that there could be a number of detectable events per year, we turn our focus to how we will need to go about detecting them.

We have seen in the previous section that PBHs cannot explain the entire DM budget in the mass range relevant for ET and CE searches. However, if they account for a subdominant fraction of the DM, they must be accompanied by a component of particle DM making up the remainder. Both analytical calculations and verifying simulations [22,23,25,97] have shown that in this scenario (cold, collisionless) DM particles will form dense spikes around PBHs with a distinct power law density profile

$$\rho(r) = \rho_{\rm sp}\left(\frac{r_{\rm sp}}{r}\right)^{\gamma_s}, \tag{14}$$

where $\gamma_s = 9/4$, $\rho_{\rm sp} = \frac{1}{2}\rho_{\rm eq}$ and $r_{\rm sp} = (2Gm_1 t_{\rm eq}^2)^{1/3}$ [97]. Here, r is the radial distance from the central PBH of mass m_1, with $\rho_{\rm eq}$ and $t_{\rm eq}$ being the background density and cosmic time at matter-radiation equality, respectively. We neglect relativistic corrections to the simple power law which occur for radii $r \sim r_{\rm isco}$ [36,98,99]. At these small radii, GW emission (rather than dynamical friction) is expected to dominate. A self-consistent description of dynamical friction and feedback in the relativistic regime is not yet available, though see Ref. [36] for estimates of the impact of post-Newtonian corrections in these systems.

It is useful to reparametrize the density profile in terms of the DM density ρ_6 at a distance $r_6 \equiv 10^{-6}$ pc from the BH, as in Ref. [16]:

$$\rho(r) = \rho_6\left(\frac{r_6}{r}\right)^{\gamma_s}. \tag{15}$$

For the purposes of parameter estimation, we treat ρ_6 as a free parameter which controls the overall normalization of the spike density. Of course, for a specific formation scenario, the benchmark value of ρ_6 will depend on m_1; equating Eqs. (14) and (15), we see that for a PBH mass m_1,

the benchmark density normalization should be $\rho_6 = 1.396 \times 10^{13} (m_1/M_\odot)^{3/4} M_\odot/\mathrm{pc}^3$.[3]

The DM density profile described above is valid assuming that PBHs form only a subdominant component of the DM in the Universe, such that there is essentially an infinite reservoir of particle DM from which to grow the isolated spikes [103]. As described in Sec. III A, however, we assume a non-negligible PBH fraction $f_{\mathrm{PBH}} \approx 0.013$, so we should verify that the spike properties are not substantially altered on scales which may be probed by GW searches. The mass enclosed in the DM spike is given by

$$M_{\mathrm{sp}}(r) = \frac{4\pi}{(3-\gamma_s)} \rho_6 (r_6)^3 \left(\frac{r}{r_6}\right)^{(3-\gamma_s)}. \tag{16}$$

We find that the mass of the DM spike enclosed in the radius r_{low} is $M_{\mathrm{sp}}(r_{\mathrm{low}}) \approx 1.4 \times 10^{-7} m_1$, where r_{low} corresponds to the separation of the binary when it enters the observation band at a frequency f_{low} (see Sec. III E). The fraction of the total particle DM mass captured in DM spikes at these small radii is therefore negligible compared to the total mass in PBHs (which themselves are a subdominant contribution to the cosmic DM density). Thus, we treat the spikes as isolated, with a density profile following Eq. (15).

If the dominant DM component is made up of canonical weakly interacting massive particle (WIMP)-like DM, then the dense DM spikes around PBHs would give rise to a large gamma-ray flux due to WIMP annihilation. Constraints from point source searches and the diffuse gamma-ray flux therefore severely limit the possibility of mixed PBH-WIMP DM scenarios [26,28,97]. However, if the remaining DM is composed of another candidate, such as axionlike particles or asymmetric WIMPs, these constraints can be evaded and these dense DM spikes may have an impact on GW searches for PBHs [18].

Gravitational wave searches in the LIGO/Virgo data have predominantly used matched filtering, where a bank of gravitational waveform templates which are calculated for a particular set of parameters are compared to the data to search for a "match" with a prespecified signal-to-noise threshold. Thus far, these gravitational waveforms have been modeled assuming that the inspiral and merger have occurred in vacuum. However, the gravitational waveform looks different if the inspiral instead occurs in nonempty space, namely a DM spike. We must, therefore, use non-vacuum waveforms to avoid missing signals in the data due to SNR loss and to avoid mischaracterizing signals, where the use of vacuum waveforms may lead to biased parameter reconstruction.

As the smaller BH moves through the spike of DM particles, they will form a wake which imparts a drag force on the BH, reducing its orbital velocity. This in turn causes the smaller BH to drop into a lower orbit more quickly than it would in vacuum. This effect is known as dynamical friction [104–106]. The inspiral happens in fewer GW cycles, causing the gravitational waveform to gradually go out of phase with respect to the vacuum case, an effect known as "dephasing." Full details of the state of the art in calculating the DM dephasing effect are given in Refs. [15,16]; here we briefly summarize the physics and our numerical approach.

Working at Newtonian order, the evolution of the binary separation r for quasicircular orbits can be described by

$$\dot{r} = -\frac{64 G^3 M m_1 m_2}{5 c^5 r^3} - \frac{8\pi G^{1/2} m_2 r^{5/2} \rho_{\mathrm{DM}}(r,t) \xi(r,t) \log\Lambda}{\sqrt{M} m_1}, \tag{17}$$

where $M = m_1 + m_2$ is the total mass of the binary. The first term on the right-hand side corresponds to GW emission, while the second corresponds to dynamical friction.[4] The dynamical friction force traces the density profile of the DM within the spike $\rho_{\mathrm{DM}}(r,t)$, while the factor $\xi(r,t)$ corresponds to the fraction of DM particles at a given radius r moving more slowly that the local orbital speed, which are those relevant for the calculation of the dynamical friction force (see Sec. 8.1 in Ref. [107]). The Coulomb logarithm $\log\Lambda$ incorporates information about the range of distances from the smaller BH at which gravitational scattering with DM particles is effective. Following Ref. [15], we take $\Lambda = \sqrt{m_1/m_2}$.

During the inspiral, the motion of the BH binary will inject energy into the DM spike, altering its density profile. In Ref. [15], the DM spike was described in terms of a spherically symmetric, isotropic distribution function, which is altered by the gravitational scattering of DM particles with the orbiting BH. Following the evolution of this distribution allows us to calculate the time evolution of the DM density and velocity distribution, $\rho_{\mathrm{DM}}(r,t)\xi(r,t)$, while simultaneously solving for the binary separation r through Eq. (17). Given a trajectory $r(t)$ the GW frequency is calculated as

$$f(t) = \frac{1}{\pi}\sqrt{\frac{GM}{r(t)^3}}, \tag{18}$$

[3]This value of ρ_6 differs slightly from that given for PBHs in Ref. [16], as we here use slightly updated cosmological parameters. In this work, we take $\rho_{\mathrm{eq}} = 2605 M_\odot/\mathrm{pc}^3$ and $t_{\mathrm{eq}} = 1.617 \times 10^{12}$ s, calculated using CAMB [100,101], assuming Planck-2018 cosmology [102].

[4]We neglect contributions from accretion onto the smaller BH and the varying enclosed mass due to the DM spike; in the absence of feedback, these effects are expected to be subdominant [9,13].

from which the strain and phase to coalescence can be calculated using Eq. (2).

The feedback formalism described above was implemented in the publicly available HaloFeedback code [108]. The most prominent effect is that the spike will be locally depleted as some particles are ejected, reducing the size of the dephasing effect. Taking into account this effect requires time-consuming numerical simulations using HaloFeedback. However, for the parameter estimation that we would like to conduct, we need to produce waveforms for a densely sampled region of the parameter space, and therefore we will rely on the analytic model that was proposed and used in Ref. [16] to describe the dephasing including feedback. In this model, the phase to coalescence $\Phi(f)$ approximately follows a broken power law, with the break frequency f_b a function of m_1, m_2 and γ_s. The functional form for $f_b(m_1, m_2, \gamma_s)$ was fit to HaloFeedback simulations of binaries with total masses in the range $M \sim 10^3$–$10^4 M_\odot$. However, as we show in Appendix B, this parametrization also provides an accurate fit to the behavior of the much lighter systems we consider here. We therefore rely on this parametrization to calculate the waveforms of light, dressed PBH binaries in the following sections.

V. ASSESSING DETECTABILITY, DISCOVERABILITY AND MEASURABILITY

In order to assess the prospects for concretely measuring DM spikes around PBHs with ground-based GW observatories, we follow the approach of Ref. [16]. Assuming Gaussian noise, the likelihood can be written as

$$p(d|h_{\boldsymbol{\theta}}) \propto \exp[\langle h_{\boldsymbol{\theta}}|d\rangle^2 - \frac{1}{2}\langle h_{\boldsymbol{\theta}}|h_{\boldsymbol{\theta}}\rangle], \tag{19}$$

where $d(t)$ is the strain time series data measured by the detector [which we assume to match the our benchmark signal $s(t)$] and $h_{\boldsymbol{\theta}}$ is a model waveform $h_{\boldsymbol{\theta}}(t)$ with parameters $\boldsymbol{\theta}$. In Eq. (19), the noise-weighted inner product is defined as

$$\langle a|b\rangle = 4\mathrm{Re}\int_0^\infty \mathrm{d}f \frac{\tilde{a}(f)^* \tilde{b}(f)}{S_n(f)}, \tag{20}$$

where $S_n(f)$ is the noise power spectral density (effectively the sensitivity curve of a given detector as a function of GW frequency). For Einstein Telescope, we assume the "ET-D" configuration [30] (with a factor of 0.816 to account for the detector's equilateral-triangle layout), making use of sensitivity estimates provided by the ET Collaboration [109]. For Cosmic Explorer, we assume the sensitivity as given in Ref. [110]. In all cases, we adopt the sensitivity averaged over sky locations, polarizations and binary orientations.

The parameters $\boldsymbol{\theta} = \boldsymbol{\theta}_{\rm int} \cup \boldsymbol{\theta}_{\rm ext}$ which describe the model waveform $h_{\boldsymbol{\theta}}$ can be divided into intrinsic parameters $\boldsymbol{\theta}_{\rm int}$, which describe the properties of the source, and extrinsic parameters $\boldsymbol{\theta}_{\rm ext}$, which depend on the observer. The intrinsic parameters describing the systems are

$$\text{vacuum:} \quad \boldsymbol{\theta}_{V,\rm int} = \{\mathcal{M}\}, \tag{21}$$

$$\text{dark dress:} \quad \boldsymbol{\theta}_{D,\rm int} = \{\gamma_s, \rho_6, \mathcal{M}, \log_{10} q\}, \tag{22}$$

where $q = m_2/m_1$ is the mass ratio of the binary.[5] Assuming the detector's response is constant over the duration of the waveform, the extrinsic parameters $\boldsymbol{\theta}_{\rm ext}$ we consider are the luminosity distance to the system and the phase and time at coalescence:

$$\boldsymbol{\theta}_{\rm ext} \equiv \{d_L, \phi_c, \tilde{t}_c\}. \tag{23}$$

In practice, at each point in parameter space, we maximize the likelihood over the extrinsic parameters using a fast Fourier transform, as described in Ref. [16]. This maximized likelihood is denoted $p_{\rm max}(d|h_{\boldsymbol{\theta}})$.

To compute the noise-weighted inner product, we integrate over the frequency range beginning a week before the system being observed coalesces and ending at the ISCO frequency. The use of this fixed frequency window introduces a subtle issue: the waveform being compared with the observation may last for more or less than a week over this frequency window. This means that it is not quite correct to maximize the noise-weighted inner product using a Fourier transform. Fixing this issue requires either numerically maximizing over $\tilde{t}_c$ or including it in the parameter estimation. We postpone further investigation to future work.

We explore the posterior distribution $p(\boldsymbol{\theta}|d) \propto p_{\rm max}(d|h_{\boldsymbol{\theta}})p(\boldsymbol{\theta})$ using nested sampling [111,112], implemented in the code DYNESTY [113]. The priors we take for the intrinsic parameters are summarized in Table I. The initial slope of the density profile around PBHs has been analytically predicted and numerically verified (e.g. [97]) as $\gamma_s = 2.25$, hence the reasonably narrow prior on this parameter, given that for these masses, we must be observing primordial black holes. We allow for a wide prior on the density normalization which includes the vacuum value and a range of mass ratios that have an upper bound of $10^{-2.5}$ where the assumptions on the survival of the spike break down. Mapping out the posteriors allows us to assess the question of *measurability*:

[5]We define the masses in the detector frame $m_{\rm det}$ related to the source-frame mass $m_{\rm src}$ by $m_{\rm det} = m_{\rm src}(1+z)$. Note that at a luminosity distance of $d_{\rm L} \sim 200$ Mpc (roughly the detectability horizon for these systems with ET and CE, as shown in Fig. 2), the redshift is $z \sim 0.05$, so we expect only a small correction distinguishing between detector- and source-frame masses.

TABLE I. Prior ranges on intrinsic parameters. In each case, we assume a uniform prior over the range given above. Since we use the same wide prior on the chirp mass for the dark dress and vacuum systems, its precise value cancels out in the Bayes factor and does not matter.

Parameter	Prior range
γ_s	[2.0, 2.5]
ρ_6 $[10^{15} M_\odot/\mathrm{pc}^3]$	[0, 2]
$\mathcal{M}$ $[M_\odot]$	...
$\log_{10} q$	[−4.5, −2.5]

how well the properties of binary with a DM dress can be measured or constrained.

In order to address the question of *discoverability* (i.e. whether a given dark dress waveform can be distinguished from a GR-in-vacuum waveform), we compute the Bayes factor for the dark dress and vacuum models, defined as the evidence ratio:

$$\mathrm{BF}(d) \equiv \frac{p(d|\mathrm{D})}{p(d|\mathrm{V})}. \tag{24}$$

The evidence for a given model is defined as

$$p(d) = \int \mathrm{d}\boldsymbol{\theta}\, p_{\max}(d|h_{\boldsymbol{\theta}}) p(\boldsymbol{\theta}), \tag{25}$$

where $\boldsymbol{\theta} = \boldsymbol{\theta}_D$ or $\boldsymbol{\theta} = \boldsymbol{\theta}_V$ for the dark dress and vacuum models, respectively. Large values of the Bayes factor (BF > 100) correspond to strong evidence in favor of a dark dress system, compared to a GR-in-vacuum system [114,115].

VI. RESULTS

A. Detectability

We find that aLIGO, ET and CE will be able to detect our benchmark system with a SNR of 12 out to a distance of 6.5, 86 and 286 Mpc, respectively (see Fig. 2). These distances together with the upper bound on the (binned) merger rate for systems with $m_1 = (1.0 \pm 0.5) M_\odot$ and $m_2 = 10^{-3} m_1$ corresponds to event rates of 1×10^{-4}, 0.2 and 9 per year. Increasing the mass of the systems would increase the distance out to which ET and CE will be able to detect the system, but the price to pay is that the merger rate decreases with larger m_1 as shown in Fig. 6.

B. Discoverability

We have evaluated the Bayes factor for a PBH binary with $(m_1, m_2) = (10, 10^{-2}) M_\odot$, assuming 1 week of observation with ET and CE. We find $\mathrm{BF} \approx 10^{18}$ for ET and $\mathrm{BF} \approx 6 \times 10^6$ for CE, indicating overwhelming evidence in favor of the presence of a dark dress in the system in both cases. For this system we also find that the dephasing with respect to the best-fit vacuum system is $\mathcal{O}(100)$ cycles.

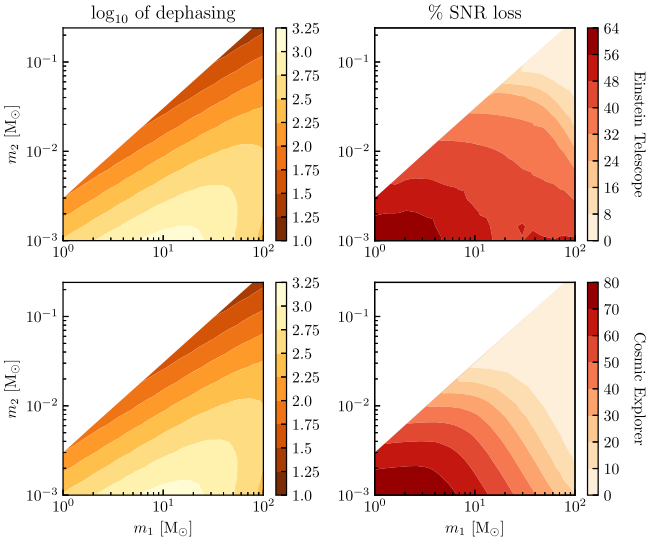

FIG. 8. Dephasing and SNR loss between best-fit vacuum template and dark dresses with various masses. The rows correspond to ET and CE. Assumes one week of observing with the system at a distance such that it is detected with an SNR of 12 by each detector.

As shown in the left panels of Fig. 8, lighter systems (including our benchmark system) than this will have an even larger dephasing [for example, exceeding 1000 cycles for $(m_1, m_2) = (10, 10^{-3}) M_\odot$]. We therefore conclude that, over the parameter space of interest for light PBHs, the presence of a dark dress should be discoverable with observation times of 1 week or more.

We also show in Fig. 8 the percentage SNR loss between the dephased system and the best-fitting vacuum system. For the system with $(m_1, m_2) = (10, 10^{-2}) M_\odot$ described above, the SNR loss is roughly 40%. This indicates that searching for dark dresses with vacuum templates will result in a large number of missed detections relative to a search based on dark dress templates. Given that the optimal matched-filtered SNR scales as d_L^{-1} [see Eq. (1)], this SNR loss would correspond to a reduction of the detectable volume for these systems $\sim d_L^3$ by a factor of $(0.6)^3 \sim 4.6$. The use of vacuum waveforms would substantially reduce the observable rate of large-mass-ratio PBH mergers. Looking again at lighter systems, the SNR loss increases further. For binaries with $(m_1, m_2) = (1, 10^{-3}) M_\odot$, the SNR loss with CE approaches 80%, reducing the observable volume by a factor ∼100, highlighting the importance of using dephased waveforms to effectively search for such systems.

C. Measurability

The one- and two-dimensional marginal posteriors for the intrinsic parameters of a dressed PBH system with benchmark masses of $m_1 = 1 M_\odot$ and $m_2 = 10^{-3} M_\odot$ observed with Einstein Telescope are shown in Fig. 9.

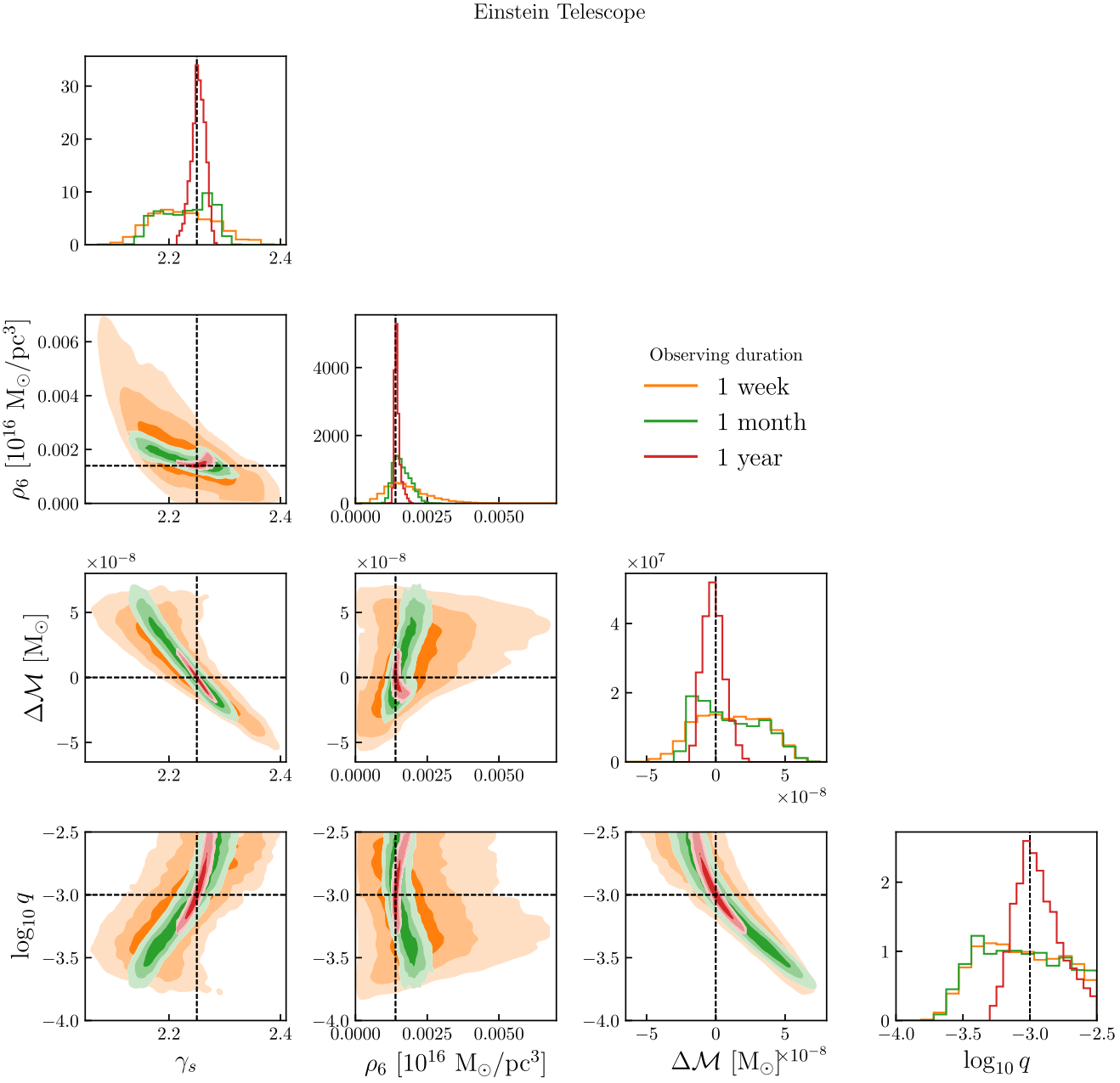

FIG. 9. One- and two-dimensional marginal posteriors for the intrinsic parameters of PBH dark dresses observed with Einstein Telescope for one week (orange), one month (green) or one year (red). The dashed black lines indicate the true parameter values. The black hole masses are set to the benchmark values of $1M_\odot$ and $10^{-3}M_\odot$, and $\Delta\mathcal{M}$ is the difference between the measured and true chirp mass ($\sim 1.585 \times 10^{-2} M_\odot$). The distances for the systems are set so each is detected with an SNR of 12. The shaded contours show the 65%, 95% and 99.7% credible regions.

The true values of the parameters are shown by the dashed black lines, and the posteriors for week-, month- and year-long signals are shown by the orange, green and red contours, respectively. With even one week's worth of data, it will be possible to measure the slope of the density profile to precision $\gamma_s = 2.22^{+0.07}_{-0.05}$,[6] and with a year's worth of data, $\gamma_s = 2.25^{0.01}_{-0.01}$. The measured values for the other parameters are given in Table II.

We run the same parameter estimation for Cosmic Explorer and find comparable errors on the parameters to Einstein Telescope in Fig. 10. We note, however, that increasing the duration of the signal from one month to one year from merger does not improve the size of the contours for Cosmic Explorer because of the low-frequency cutoff of the noise curve—see Fig. 1.

[6]We use error bars indicating the 68% credible interval.

TABLE II. Parameters inferred for benchmark system with one week of observations by different detectors. The error bars indicate the 68% credible intervals.

Parameter	Einstein telescope	Cosmic explorer
γ_s	$2.22^{+0.07}_{-0.05}$	$2.20^{+0.07}_{-0.06}$
ρ_6 $[10^{13} M_\odot/\mathrm{pc}^3]$	$1.7^{+0.8}_{-0.6}$	$2.0^{+1}_{-0.8}$
$\mathcal{M}$ $[M_\odot]$	$1\,584\,577^{+3}_{-3} \times 10^{-8}$	$1\,584\,578^{+3}_{-3} \times 10^{-8}$
$\log_{10}(q)$	$-3.1^{+0.4}_{-0.3}$	$-3.2^{0.4}_{-0.3}$

In Fig. 11 we highlight the one-dimensional marginal posteriors for ρ_6 and γ_s to show the precision with which we can measure these parameters, as well as the improvement from increasing the duration of the signal. We stress, however, that one week's worth of data will be enough to measure these parameters with a few percent accuracy and presents a less daunting data analysis challenge than year-long signals.

So far, we have included all of the intrinsic parameters of the system in the parameter estimation pipeline,

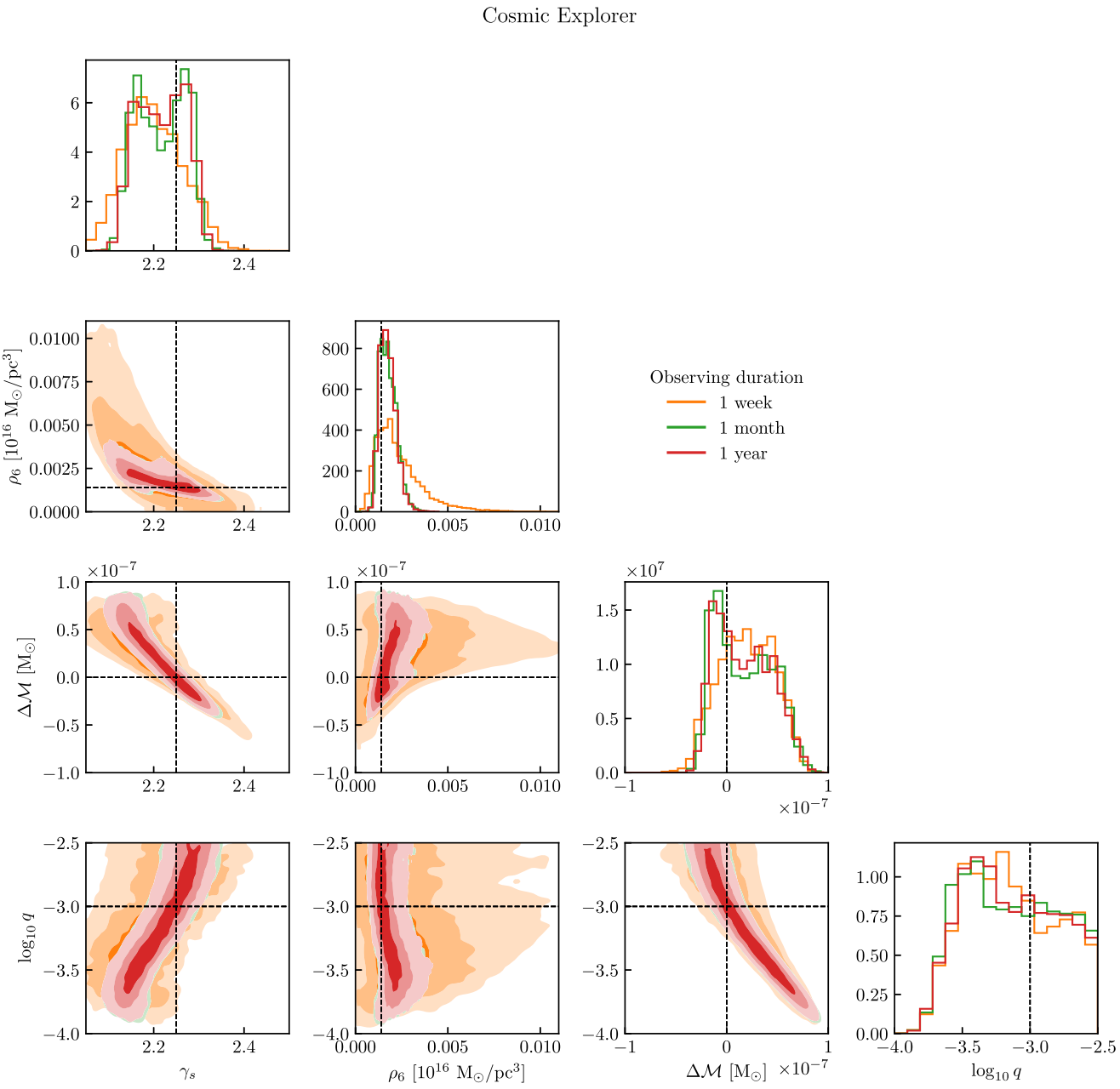

FIG. 10. Marginal posteriors for a PBH dark dress as in Fig. 9, but instead observed with Cosmic Explorer. The system's distance was set to give an SNR of 12 at CE.

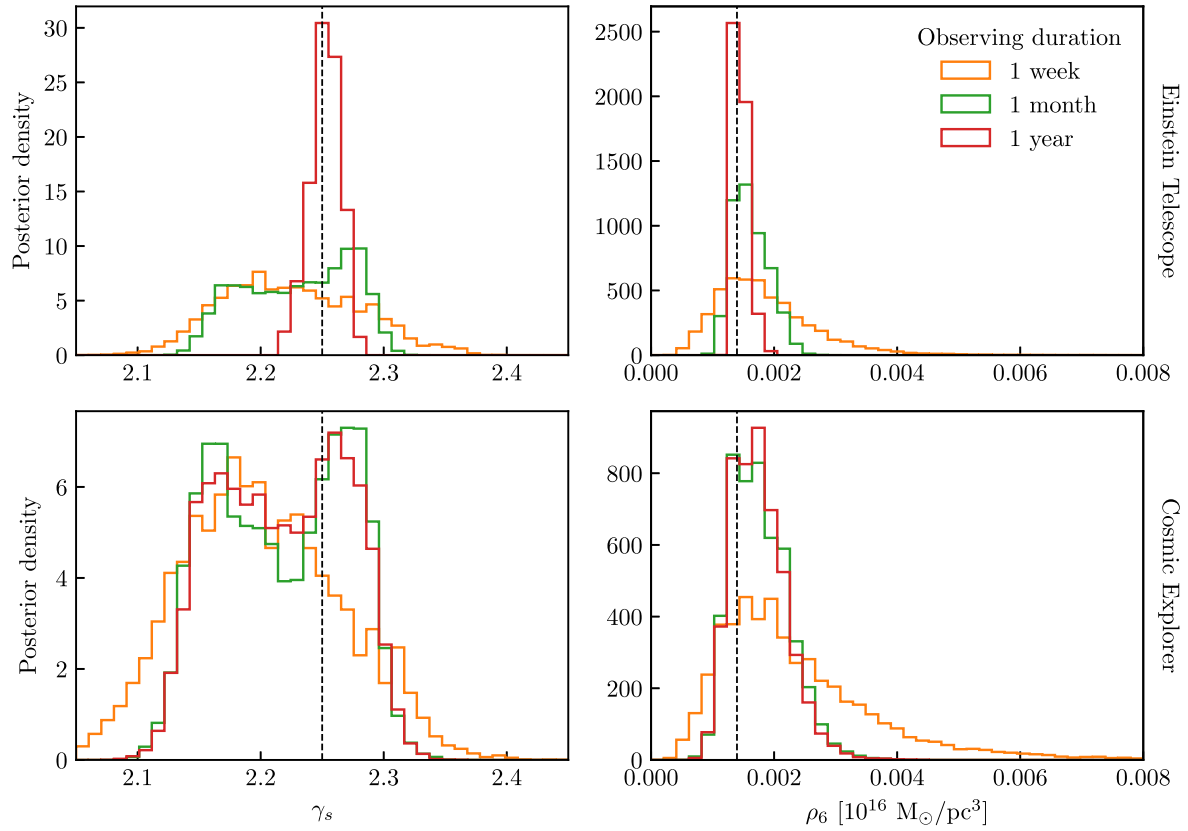

FIG. 11. The 1D marginal posteriors for ρ_6 and γ_s obtained using Einstein Telescope and Cosmic Explorer. Note the target dark dress systems in the two rows are *not* the same. Their distances differ since each is observed with an SNR of 12 in its respective detector.

specifically $\{\gamma_s, \rho_6, \mathcal{M}, \log_{10} q\}$. However, for PBH systems, the value of γ_s is fixed and the density normalization ρ_6 is uniquely determined by the central PBH mass, as described in Sec. IV. Assuming a PBH origin for the dephasing signal therefore allows us to reduce the parameter estimation problem to two dimensions—$\{\rho_6, \mathcal{M}\}$—which substantially strengthens constraints, as we describe in Appendix C.

VII. DISCUSSION

We have explored the prospects for detecting the presence of DM spikes around light PBH binaries with future ground-based GW observatories, such as ET and CE. We focus on a broad, well-motivated PBH mass function with $f_{\rm PBH} \approx 0.013$, which is still allowed by current constraints from microlensing and the stochastic GW background.

We can expect between 300 and 2400 PBH mergers per Gpc^3 volume per year and an event rate for our specific benchmark system of $m_1 = 1 \pm 0.5 M_\odot$, $m_2 = 10^{-3} m_1$, of 0.2 and 9 events per year, observable with an SNR of at least 12 in each of ET and CE, respectively. We note that if ET and CE are online simultaneously, the SNR threshold for each individual detector could be lowered, and hence the distance at which PBH mergers of a given mass are observable increases along with the event rate.

We find that, for our benchmark system, the SNR lost if the waveform is matched with a vacuum template could be as large as 80%. This suggests that search strategies will need to take into account the effect of the DM spikes so as to avoid missing these signals. For larger m_1 than our benchmark system, the SNR loss will be smaller, so the system may be detectable with vacuum templates but would lead to biased parameter inference.

We show that using the correct model for parameter estimation, i.e. including the effects of the dark matter spike on the waveform, we can reconstruct the intrinsic parameters of the binary, the chirp mass and the mass ratio, as well as the parameters of the spike, the density normalization and the power law of the dark matter density profile, to very good precision with one week's worth of data, as summarized in Table II.

We find that Einstein Telescope can measure the dark matter spike parameters with better precision than Cosmic Explorer, owing to the lower frequency reach, which allows

more cycles to be observed and hence more dephasing to accumulate. We note that there may be opportunities for multiband observations of systems that overlap with the frequency ranges of both LISA and ET or CE [116].

Since PBH binaries of these masses and mass ratios must be embedded in DM spikes (assuming they cannot make up all of the dark matter themselves), we conclude that, in order to find these systems and measure their parameters correctly, the effect of dark matter on the phase of the inspiral must be taken into account in at least the parameter estimation process to avoid biased parameter inference. For some ranges of the parameter space (for example our benchmark system), the effect of the dark matter must be taken into account in order to detect the signal in the first place, as the SNR loss incurred by assuming the system is inspiralling in vacuum could be catastrophic.

We also emphasize that less extreme-mass-ratio mergers will also exist for our PBH formation scenario, which should be inspiralling in vacuum, since we expect their dark matter spikes to have been disrupted. Observations of these systems (potentially even with aLIGO/Virgo [93,94]) would be a very strong indicator that the more extreme-mass-ratio systems are out there to be found and would provide strong motivation for conducting a search for these exotic waveforms in the data.

These conclusions are drawn assuming that the search and inference will be conducted using matched filtering with template banks. However, considering the duration of the signals expected, techniques from continuous wave searches [117] may be more suitable for searching for these signals that go through millions of cycles. Recently, Ref. [118] proposed the use of the Hough transform to search for "mini-EMRIs," systems similar to those we consider here. The authors estimate that for a strain sensitivity similar to that of LIGO, a binary with masses $(10, 10^{-2})M_\odot$ may be detectable out to a distance of a few Mpc with this technique. This is roughly a factor of 2 less than the detectable distance we estimate in Fig. 2, suggesting that the application of more realistic search strategies need not substantially degrade the detectability of the signals.

In any case, it will be vital to understand the evolution of the frequency as a function of time for these systems and how it differs from the vacuum case. There is also potential for the use of machine learning to search the data for such long duration signals, in order to decrease the expense of computing the (many thousands of) waveforms of these systems directly.

While we have focused here on DM spikes around PBH binaries, many of the tools and conclusions apply also to other environmental effects. These include binaries embedded in accretion disks [119] or "gravitational atoms" (clouds of light scalar fields bound to BHs) [120–122]. For these systems, too, future ground-based observatories will provide exquisite sensitivity to slowly accumulating dephasing effects. Our results suggest that $\mathcal{O}(\text{weeks})$ of data would be required to extract useful physical information from such systems, though a detailed study of this—and of whether the environmental effects from these different sources can be distinguished—we leave for future work.

ACKNOWLEDGMENTS

We thank Thomas Edwards, Andrew Gow, Samaya Nissanke and Ville Vaskonen for useful conversations. P. S. C. acknowledges funding from the Institute of Physics, University of Amsterdam. A. C. received funding from the Netherlands eScience Center (Grant No. ETEC.2019.018) and the Schmidt Futures Foundation. B. J. K. thanks the Spanish Agencia Estatal de Investigación (AEI, Ministerio de Ciencia, Innovación y Universidades) for the support to the Unidad de Excelencia María de Maeztu Instituto de Física de Cantabria, Ref. No. MDM-2017-0765. We acknowledge Santander Supercomputing support group at the University of Cantabria who provided access to the supercomputer Altamira at the Institute of Physics of Cantabria (IFCA-CSIC), member of the Spanish Supercomputing Network, for performing simulations and analyses.

APPENDIX A: GW SPECTRUM FROM COALESCING BHs

For the interested reader, we here give explicitly expressions for the GW spectrum of coalescing black holes, which appears in the calculation of the stochastic GW background in Sec. III C.

The energy emitted by coalescing BHs with masses m_1 and m_2 in the GW frequency range $[f, f + \mathrm{d}f]$ is given by [87,123,124]

$$\frac{\mathrm{d}E_{\mathrm{GW}}}{\mathrm{d}f} = \mathcal{C}\begin{cases} f^{-\frac{1}{3}} & \text{for } f < f_1, \\ \frac{f^{\frac{2}{3}}}{f_1} & \text{for } f_1 \le f < f_2, \\ \frac{f f_3^4}{(f_1 f_2^{\frac{4}{3}}(4(f-f_2)^2+f_4)^2)^2} & \text{for } f_2 \le f < f_3, \\ 0 & \text{for } f_3 \le f < f_4, \end{cases}$$

where the prefactor is $\mathcal{C} = (\pi G)^{\frac{2}{3}} M^{\frac{5}{3}} \eta$. The frequency window limits are given numerically by [125]

$$f_j = \frac{(a_j \eta^2 + b_j \eta + c_j) c^3}{\pi G (m_1 + m_2)}, \tag{A1}$$

where e.g. a_j denotes the jth index of the following arrays:

$$a = (0.2971, 0.59411, 0.84845, 0.50801), \quad \text{(A2)}$$

$$b = (0.04481, 0.089794, 0.12848, 0.077515), \quad \text{(A3)}$$

$$c = (0.095560, 0.19111, 0.27299, 0.022369), \quad \text{(A4)}$$

and $\eta = m_1 m_2/(m_1 + m_2)^2$.

APPENDIX B: HaloFeedback VALIDATION

Here, we present some validation tests which were performed for the $f(t)$ parametrization presented in Ref. [16] and used in Sec. V of this work.

We begin by checking that the formalism developed in Ref. [15] behaves well for the low BH masses we consider here. In Fig. 12, we show the effective density profile extracted from simultaneously evolving the separation of the PBH binary and the DM spike distribution function (as summarized in Sec. IV and implemented in the HaloFeedback code [108]). The effective density is the instantaneous DM density experienced by the smaller inspiralling BH when it reaches an orbital separation r. For reference, the orbital reference corresponding to the break frequency f_b for this system is shown as a vertical dotted line.

The qualitative behavior of the effective density matches that observed in the heavier systems presented in Ref. [16]. Because of energy injected by the BH into the spike, the spike is rapidly depleted and thus the effective density is smaller than the initial, unperturbed density (gray dashed line). As the GW inspiral continues (from large r to small r), the timescale for depletion of the spike eventually becomes longer than the timescale for the GW inspiral, and the effective density converges to the initial unperturbed profile. Lines of different colors in Fig. 12 correspond to simulations which were started at different initial BH separations. After an initial depletion phase, each of these density profiles converges to the same behavior, indicating that we do not need to explicitly specify the initial separation of the binary at formation (as long as this is larger than the radius at which the binary enters the GW observing band).

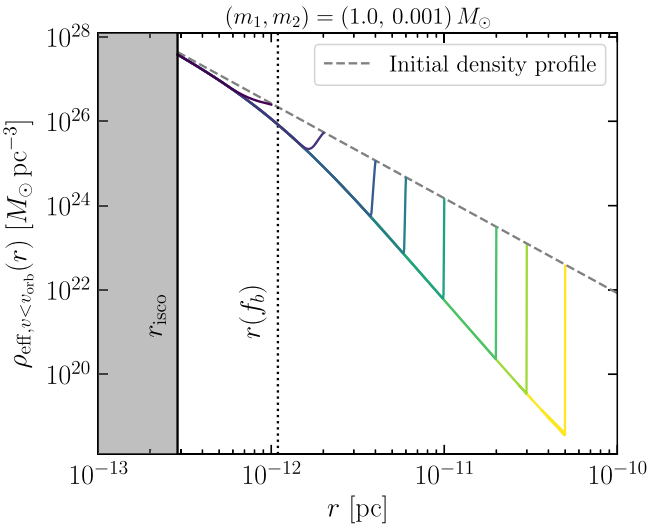

FIG. 12. Effective density profile of the DM spike, obtained using HaloFeedback. Each colored line corresponds to a simulation beginning at a different initial PBH binary separation, while the diagonal dashed line shows the unperturbed DM density profile. The behavior of the system at small radii is independent of the initial separation.

Having verified that the behavior of HaloFeedback is sensible for these light systems, we can now compare these simulations against the phase parametrization $\Phi(f)$ which we use for parameter estimation in this work. From the trajectories obtained in these simulations, we can calculate the evolution of the GW phase with frequency and compare this with the corresponding predictions from the analytic phase parametrization. In Fig. 13, we plot the dephasing with respect to the vacuum case for PBH binaries

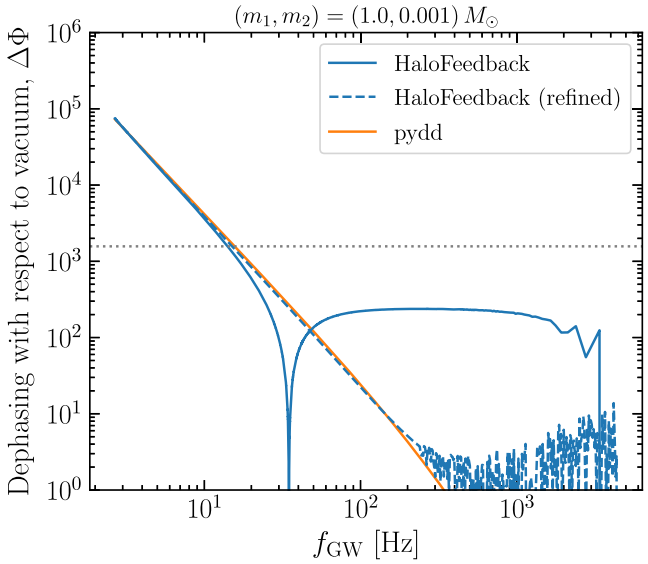

FIG. 13. DM-induced dephasing with respect to the vacuum for different modeling approaches. The solid blue line shows the dephasing modeled using the HaloFeedback code [108], solving simultaneously the inspiral and feedback on the DM spike. For computational ease, the maximum step size is set to 100 orbits (corresponding to a phase given by the horizontal dotted line). The dashed blue line is obtained assuming a static DM spike with effective density profile extracted from the full HaloFeedback run, allowing for a shorter time step. This matches closely the output of PYDD [126] (solid orange line), which implements the analytic fit to the phase $\Phi(f)$ used in Sec. V of this work and first presented in Ref. [16].

with masses $(m_1, m_2) = (1.0, 10^{-3})M_\odot$. The full HaloFeedback simulations are shown in solid blue, using a maximum time step of 100 orbits (corresponding to a phase given by the horizonal dotted line). We use this simulation to extract the effective DM density profile and resimulate assuming a *static* spike with this density profile. This allows us to substantially reduce the maximum time step and therefore resolve the dephasing much closer to the merger (dashed blue line). These results are matched closely by the output of the analytical parametrization, as implemented in PYDD [126], down to the level of a few cycles.

Despite being calibrated on BH masses a few orders of magnitude larger than those being considered here, the analytic parametrization maintains percent-level accuracy over many years of the inspiral. We have also verified this behavior for various mass ratios and total masses of the light PBH systems.

APPENDIX C: POSTERIORS FOR FIXED γ_s

In the main body of the paper, we have performed parameter estimation for all four intrinsic parameters of the dark dress systems: γ_s, ρ_6, $\mathcal{M}$ and q. However, it is also interesting in the case of PBHs to make use of the fact that there is a concrete prediction for the slope of the spike $\gamma_s = 9/4$, as well as that ρ_6 is directly related to the mass of the primary black hole m_1. With this in mind, we fix $\gamma_s = 9/4$ and perform inference over the parameters ρ_6 and $\mathcal{M}$, using Eqs. (14) and (15) to fix the mass ratio q. This is a strong assumption on two fronts: firstly it assumes that the system is definitely primordial (reasonable if the primary mass is below $1.4M_\odot$) and that the predictions from analytic calculations and simulations are correct and have no scatter, and secondly it assumes that the spike has not been at all disrupted down to redshifts less than one, such that the density profile slope and relationship between the normalization and m_1 remains intact. While we do not foresee this type of parameter estimation being implemented for the discovery of the first system of this type, it demonstrates how well we can predict the parameters of the system if we are confident that we are observing one of a (perhaps previously confirmed) population of primordial black holes with preexisting evidence that the density profile slope of these systems is $\gamma_s = 9/4$.

The resulting posteriors are shown in Fig. 14 for an analysis with Einstein Telescope and in Fig. 15 for an analysis with Cosmic Explorer. Unsurprisingly, in both cases the posteriors are extremely narrow even with just one day of observations before coalescence. The chirp mass can be measured to within approximately 3×10^{-9} of the true value, and the density normalization ρ_6 to better than 1% precision with 99.7% confidence.

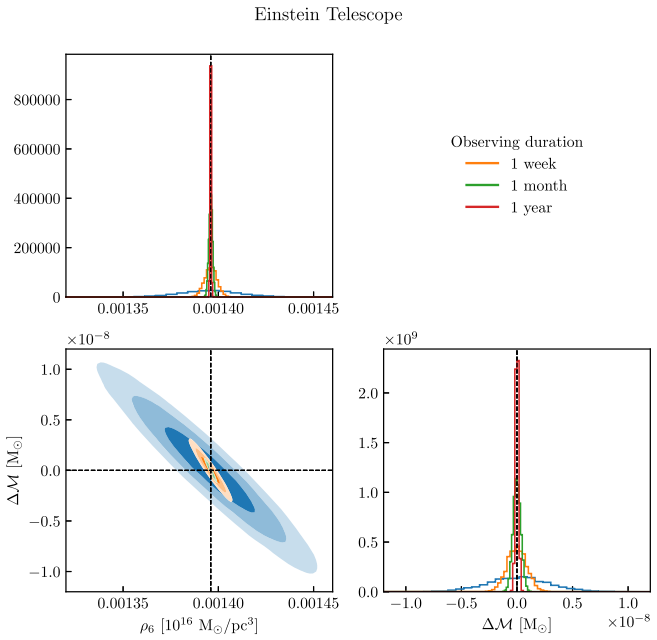

FIG. 14. One- and two-dimensional marginal posteriors for a subset of the intrinsic parameters of PBH dark dresses, keeping γ_s and q fixed, observed with Einstein Telescope for times ranging from one week to one year. The dashed black lines indicate the true parameter values. The black hole masses are set to the benchmark values of $1M_\odot$ and $10^{-3}M_\odot$, and $\Delta\mathcal{M}$ is the difference between the measured and true chirp mass ($\sim 1.585 \times 10^{-2}M_\odot$). The distances for the systems are set so each is detected with an SNR of 12. The contours indicate the 65%, 95% and 99.7% credible regions.

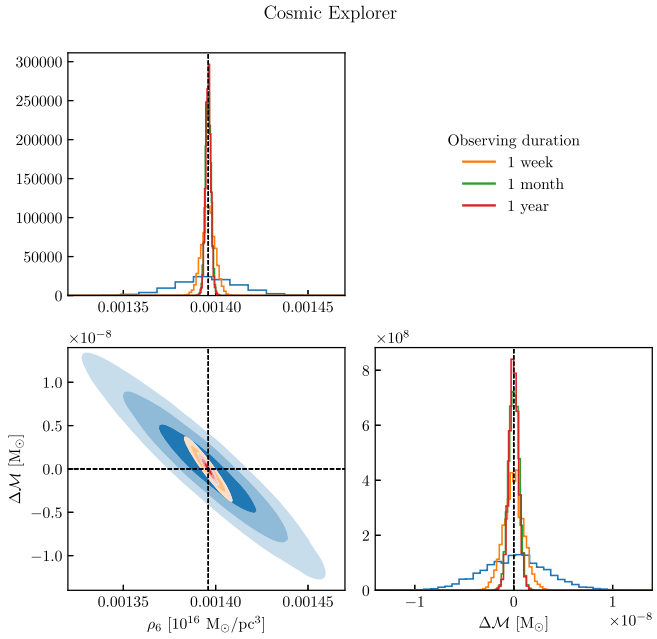

FIG. 15. Marginal posteriors for a PBH dark dress with γ_s and q fixed as in Fig. 14 but instead observed with Cosmic Explorer.

[1] E. Hall, Horizon plots and noise curves for second- and third-generation detectors, LIGO document T1800084-v5, https://dcc.ligo.org/LIGO-T1800084-v5/public (2019).
[2] M. Punturo *et al.*, The Einstein Telescope: A third-generation gravitational wave observatory, Classical Quantum Gravity **27**, 194002 (2010).
[3] Michele Maggiore *et al.*, Science case for the Einstein Telescope, J. Cosmol. Astropart. Phys. 03 (2020) 050.
[4] Matthew Evans *et al.*, A horizon study for cosmic explorer: Science, observatories, and community, arXiv: 2109.09882.
[5] Leor Barack *et al.*, Black holes, gravitational waves and fundamental physics: A roadmap, Classical Quantum Gravity **36**, 143001 (2019).
[6] Gianfranco Bertone *et al.*, Gravitational wave probes of dark matter: Challenges and opportunities, SciPost Phys. Core **3**, 007 (2020).
[7] Kazunari Eda, Yousuke Itoh, Sachiko Kuroyanagi, and Joseph Silk, New Probe of Dark-Matter Properties: Gravitational Waves from an Intermediate-Mass Black Hole Embedded in a Dark-Matter Minispike, Phys. Rev. Lett. **110**, 221101 (2013).
[8] Kazunari Eda, Yousuke Itoh, Sachiko Kuroyanagi, and Joseph Silk, Gravitational waves as a probe of dark matter minispikes, Phys. Rev. D **91**, 044045 (2015).
[9] Caio F. B. Macedo, Paolo Pani, Vitor Cardoso, and Luís C. B. Crispino, Into the lair: Gravitational-wave signatures of dark matter, Astrophys. J. **774**, 48 (2013).
[10] Enrico Barausse, Vitor Cardoso, and Paolo Pani, Can environmental effects spoil precision gravitational-wave astrophysics?, Phys. Rev. D **89**, 104059 (2014).
[11] Enrico Barausse, Vitor Cardoso, and Paolo Pani, Environmental effects for gravitational-wave astrophysics, J. Phys. Conf. Ser. **610**, 012044 (2015).
[12] Xiao-Jun Yue and Wen-Biao Han, Gravitational waves with dark matter minispikes: The combined effect, Phys. Rev. D **97**, 064003 (2018).
[13] Vitor Cardoso and Andrea Maselli, Constraints on the astrophysical environment of binaries with gravitational-wave observations, Astron. Astrophys. **644**, A147 (2020).
[14] Otto A. Hannuksela, Kenny C. Y. Ng, and Tjonnie G. F. Li, Extreme dark matter tests with extreme mass ratio inspirals, Phys. Rev. D **102**, 103022 (2020).
[15] Bradley J. Kavanagh, David A. Nichols, Gianfranco Bertone, and Daniele Gaggero, Detecting dark matter around black holes with gravitational waves: Effects of dark-matter dynamics on the gravitational waveform, Phys. Rev. D **102**, 083006 (2020).
[16] Adam Coogan, Gianfranco Bertone, Daniele Gaggero, Bradley J. Kavanagh, and David A. Nichols, Measuring the dark matter environments of black hole binaries with gravitational waves, Phys. Rev. D **105**, 043009 (2022).
[17] David Merritt, Milos Milosavljevic, Licia Verde, and Raul Jimenez, Dark Matter Spikes and Annihilation Radiation from the Galactic Center, Phys. Rev. Lett. **88**, 191301 (2002).
[18] Bradley J. Kavanagh, Daniele Gaggero, and Gianfranco Bertone, Merger rate of a subdominant population of primordial black holes, Phys. Rev. D **98**, 023536 (2018).
[19] Anne M. Green and Bradley J. Kavanagh, Primordial black holes as a dark matter candidate, J. Phys. G **48**, 043001 (2021).
[20] Sébastien Clesse and Juan García-Bellido, The clustering of massive primordial black holes as dark matter: Measuring their mass distribution with Advanced LIGO, Phys. Dark Universe **15**, 142 (2017).
[21] Sam Young and Christian T. Byrnes, Initial clustering and the primordial black hole merger rate, J. Cosmol. Astropart. Phys. 03 (2020) 004.
[22] E. Bertschinger, Self-similar secondary infall and accretion in an Einstein-de Sitter universe, Astrophys. J. Suppl. Ser. **58**, 39 (1985).
[23] Katherine J. Mack, Jeremiah P. Ostriker, and Massimo Ricotti, Growth of structure seeded by primordial black holes, Astrophys. J. **665**, 1277 (2007).
[24] Massimo Ricotti, Bondi accretion in the early universe, Astrophys. J. **662**, 53 (2007).
[25] Mathieu Boudaud, Thomas Lacroix, Martin Stref, Julien Lavalle, and Pierre Salati, In-depth analysis of the clustering of dark matter particles around primordial black holes. Part I. Density profiles, J. Cosmol. Astropart. Phys. 08 (2021) 053.
[26] Brian C. Lacki and John F. Beacom, Primordial black holes as dark matter: Almost all or almost nothing, Astrophys. J. Lett. **720**, L67 (2010).
[27] Julian Adamek, Christian T. Byrnes, Mateja Gosenca, and Shaun Hotchkiss, WIMPs and stellar-mass primordial black holes are incompatible, Phys. Rev. D **100**, 023506 (2019).
[28] Gianfranco Bertone, Adam M. Coogan, Daniele Gaggero, Bradley J. Kavanagh, and Christoph Weniger, Primordial black holes as silver bullets for new physics at the weak scale, Phys. Rev. D **100**, 123013 (2019).
[29] Bernard Carr, Florian Kuhnel, and Luca Visinelli, Black holes and WIMPs: All or nothing or something else, Mon. Not. R. Astron. Soc. **506**, 3648 (2021).
[30] S. Hild *et al.*, Sensitivity studies for third-generation gravitational wave observatories, Classical Quantum Gravity **28**, 094013 (2011).
[31] C. J. Moore, R. H. Cole, and C. P. L. Berry, Gravitational-wave sensitivity curves, Classical Quantum Gravity **32**, 015014 (2015).
[32] Xiao-Jun Yue, Wen-Biao Han, and Xian Chen, Dark matter: An efficient catalyst for intermediate-mass-ratio-inspiral events, Astrophys. J. **874**, 34 (2019).
[33] Ning Dai, Yungui Gong, Tong Jiang, and Dicong Liang, Intermediate mass-ratio inspirals with dark matter minispike, Phys. Rev. D **106**, 064003 (2022).
[34] Gen-Liang Li, Yong Tang, and Yue-Liang Wu, Probing dark matter spikes via gravitational waves of extreme mass ratio inspirals, Sci. China Phys. Mech. Astron. **65**, 100412 (2022).
[35] Niklas Becker, Laura Sagunski, Lukas Prinz, and Saeed Rastgoo, Circularization versus eccentrification in intermediate mass ratio inspirals inside dark matter spikes, Phys. Rev. D **105**, 063029 (2022).
[36] Nicholas Speeney, Andrea Antonelli, Vishal Baibhav, and Emanuele Berti, The impact of relativistic corrections on

the detectability of dark-matter spikes with gravitational waves, Phys. Rev. D **106**, 044027 (2022).
[37] Michele Maggiore, *Gravitational Waves. Vol. 1: Theory and Experiments*, Oxford Master Series in Physics (Oxford University Press, Oxford, 2007).
[38] Sergey Pilipenko, Maxim Tkachev, and Pavel Ivanov, Evolution of a primordial binary black hole due to interaction with cold dark matter and the formation rate of gravitational wave events, Phys. Rev. D **105**, 123504 (2022).
[39] V. De Luca, G. Franciolini, P. Pani, and A. Riotto, Constraints on primordial black holes: The importance of accretion, Phys. Rev. D **102**, 043505 (2020).
[40] Caner Ünal, Ely D. Kovetz, and Subodh P. Patil, Multi-messenger probes of inflationary fluctuations and primordial black holes, Phys. Rev. D **103**, 063519 (2021).
[41] Sébastien Clesse and Juan García-Bellido, The clustering of massive primordial black holes as dark matter: Measuring their mass distribution with Advanced LIGO, Phys. Dark Universe **15**, 142 (2017).
[42] Guillermo Ballesteros, Pasquale D. Serpico, and Marco Taoso, On the merger rate of primordial black holes: Effects of nearest neighbours distribution and clustering, J. Cosmol. Astropart. Phys. 10 (2018) 043.
[43] Torsten Bringmann, Paul Frederik Depta, Valerie Domcke, and Kai Schmidt-Hoberg, Towards closing the window of primordial black holes as dark matter: The case of large clustering, Phys. Rev. D **99**, 063532 (2019).
[44] Vicente Atal, Albert Sanglas, and Nikolaos Triantafyllou, LIGO/Virgo black holes and dark matter: The effect of spatial clustering, J. Cosmol. Astropart. Phys. 11 (2020) 036.
[45] S. W. Hawking, Black holes from cosmic strings, Phys. Lett. B **231**, 237 (1989).
[46] Alexander Polnarev and Robert Zembowicz, Formation of primordial black holes by cosmic strings, Phys. Rev. D **43**, 1106 (1991).
[47] Matt Crawford and David N. Schramm, Spontaneous generation of density perturbations in the early Universe, Nature (London) **298**, 538 (1982).
[48] S. W. Hawking, I. G. Moss, and J. M. Stewart, Bubble collisions in the very early Universe, Phys. Rev. D **26**, 2681 (1982).
[49] Hideo Kodama, Misao Sasaki, and Katsuhiko Sato, Abundance of primordial holes produced by cosmological first order phase transition, Prog. Theor. Phys. **68**, 1979 (1982).
[50] Vicente Atal and Cristiano Germani, The role of non-Gaussianities in primordial black hole formation, Phys. Dark Universe **24**, 100275 (2019).
[51] Christian T. Byrnes, Philippa S. Cole, and Subodh P. Patil, Steepest growth of the power spectrum and primordial black holes, J. Cosmol. Astropart. Phys. 06 (2019) 028.
[52] Andrew D. Gow, Christian T. Byrnes, Philippa S. Cole, and Sam Young, The power spectrum on small scales: Robust constraints and comparing PBH methodologies, J. Cosmol. Astropart. Phys. 02 (2021) 002.
[53] Bernard Carr, Sebastien Clesse, Juan Garcia-Bellido, and Florian Kuhnel, Cosmic conundra explained by thermal history and primordial black holes, Phys. Dark Universe **31**, 100755 (2021).
[54] Christian T. Byrnes, Mark Hindmarsh, Sam Young, and Michael R. S. Hawkins, Primordial black holes with an accurate QCD equation of state, J. Cosmol. Astropart. Phys. 08 (2018) 041.
[55] Alba Kalaja, Nicola Bellomo, Nicola Bartolo, Daniele Bertacca, Sabino Matarrese, Ilia Musco, Alvise Raccanelli, and Licia Verde, From primordial black holes abundance to primordial curvature power spectrum (and back), J. Cosmol. Astropart. Phys. 10 (2019) 031.
[56] Ilia Musco, Threshold for primordial black holes: Dependence on the shape of the cosmological perturbations, Phys. Rev. D **100**, 123524 (2019).
[57] Sam Young, Ilia Musco, and Christian T. Byrnes, Primordial black hole formation and abundance: Contribution from the non-linear relation between the density and curvature perturbation, J. Cosmol. Astropart. Phys. 11 (2019) 012.
[58] Masahiro Kawasaki and Hiromasa Nakatsuka, Effect of nonlinearity between density and curvature perturbations on the primordial black hole formation, Phys. Rev. D **99**, 123501 (2019).
[59] V. De Luca, G. Franciolini, A. Kehagias, M. Peloso, A. Riotto, and C. Ünal, The ineludible non-Gaussianity of the primordial black hole abundance, J. Cosmol. Astropart. Phys. 07 (2019) 048.
[60] Sam Young and Christian T. Byrnes, Initial clustering and the primordial black hole merger rate, J. Cosmol. Astropart. Phys. 03 (2020) 004.
[61] Gert Hütsi, Martti Raidal, Ville Vaskonen, and Hardi Veermäe, Two populations of LIGO-Virgo black holes, J. Cosmol. Astropart. Phys. 03 (2021) 068.
[62] V. De Luca, G. Franciolini, and A. Riotto, Constraining the initial primordial black hole clustering with CMB distortion, Phys. Rev. D **104**, 063526 (2021).
[63] Takashi Nakamura, Misao Sasaki, Takahiro Tanaka, and Kip S. Thorne, Gravitational waves from coalescing black hole MACHO binaries, Astrophys. J. Lett. **487**, L139 (1997).
[64] Kunihito Ioka, Takeshi Chiba, Takahiro Tanaka, and Takashi Nakamura, Black hole binary formation in the expanding universe: Three body problem approximation, Phys. Rev. D **58**, 063003 (1998).
[65] Yacine Ali-Haïmoud, Ely D. Kovetz, and Marc Kamionkowski, Merger rate of primordial black-hole binaries, Phys. Rev. D **96**, 123523 (2017).
[66] Martti Raidal, Christian Spethmann, Ville Vaskonen, and Hardi Veermäe, Formation and evolution of primordial black hole binaries in the early universe, J. Cosmol. Astropart. Phys. 09 (2019) 018.
[67] Lang Liu, Zong-Kuan Guo, and Rong-Gen Cai, Effects of the surrounding primordial black holes on the merger rate of primordial black hole binaries, Phys. Rev. D **99**, 063523 (2019).
[68] Simeon Bird, Ilias Cholis, Julian B. Muñoz, Yacine Ali-Haïmoud, Marc Kamionkowski, Ely D. Kovetz, Alvise Raccanelli, and Adam G. Riess, Did LIGO Detect Dark Matter?, Phys. Rev. Lett. **116**, 201301 (2016).
[69] Valeriya Korol, Ilya Mandel, M. Coleman Miller, Ross P. Church, and Melvyn B. Davies, Merger rates in primordial

black hole clusters without initial binaries, Mon. Not. R. Astron. Soc. **496**, 994 (2020).
[70] Gabriele Franciolini, Konstantinos Kritos, Emanuele Berti, and Joseph Silk, Primordial black hole mergers from three-body interactions, Phys. Rev. D **106**, 083529 (2022).
[71] Martti Raidal, Christian Spethmann, Ville Vaskonen, and Hardi Veermäe, Formation and evolution of primordial black hole binaries in the early universe, J. Cosmol. Astropart. Phys. 02 (2019) 018.
[72] Gert Hütsi, Martti Raidal, Ville Vaskonen, and Hardi Veermäe, Two populations of LIGO-Virgo black holes, J. Cosmol. Astropart. Phys. 03 (2021) 068.
[73] Khun Sang Phukon, Gregory Baltus, Sarah Caudill, Sebastien Clesse, Antoine Depasse, Maxime Fays, Heather Fong, Shasvath J. Kapadia, Ryan Magee, and Andres Jorge Tanasijczuk, The hunt for sub-solar primordial black holes in low mass ratio binaries is open, arXiv:2105.11449.
[74] Ville Vaskonen and Hardi Veermäe, Lower bound on the primordial black hole merger rate, Phys. Rev. D **101**, 043015 (2020).
[75] V. De Luca, V. Desjacques, G. Franciolini, and A. Riotto, The clustering evolution of primordial black holes, J. Cosmol. Astropart. Phys. 11 (2020) 028.
[76] Maxim Tkachev, Sergey Pilipenko, and Gustavo Yepes, Dark matter simulations with primordial black holes in the early Universe, Mon. Not. R. Astron. Soc. **499**, 4854 (2020).
[77] Andrew D. Gow, Christian T. Byrnes, Alex Hall, and John A. Peacock, Primordial black hole merger rates: Distributions for multiple LIGO observables, J. Cosmol. Astropart. Phys. 01 (2020) 031.
[78] V. De Luca, G. Franciolini, P. Pani, and A. Riotto, Primordial black holes confront LIGO/Virgo data: Current situation, J. Cosmol. Astropart. Phys. 06 (2020) 044.
[79] Alex Hall, Andrew D. Gow, and Christian T. Byrnes, Bayesian analysis of LIGO-Virgo mergers: Primordial versus astrophysical black hole populations, Phys. Rev. D **102**, 123524 (2020).
[80] Juan García-Bellido, José Francisco Nuño Siles, and Ester Ruiz Morales, Bayesian analysis of the spin distribution of LIGO/Virgo black holes, Phys. Dark Universe **31**, 100791 (2021).
[81] Kaze W. K. Wong, Gabriele Franciolini, Valerio De Luca, Vishal Baibhav, Emanuele Berti, Paolo Pani, and Antonio Riotto, Constraining the primordial black hole scenario with Bayesian inference and machine learning: The GWTC-2 gravitational wave catalog, Phys. Rev. D **103**, 023026 (2021).
[82] V. De Luca, G. Franciolini, P. Pani, and A. Riotto, Bayesian Evidence for both astrophysical and primordial black holes: Mapping the GWTC-2 catalog to third-generation detectors, J. Cosmol. Astropart. Phys. 05 (2021) 003.
[83] Gabriele Franciolini, Vishal Baibhav, Valerio De Luca, Ken K. Y. Ng, Kaze W. K. Wong, Emanuele Berti, Paolo Pani, Antonio Riotto, and Salvatore Vitale, Searching for a subpopulation of primordial black holes in LIGO-Virgo gravitational-wave data, Phys. Rev. D **105**, 083526 (2022).
[84] Zu-Cheng Chen, Chen Yuan, and Qing-Guo Huang, Confronting the primordial black hole scenario with the gravitational-wave events detected by LIGO-Virgo, Phys. Lett. B **829**, 137040 (2022).
[85] Bradley J. Kavanagh, PBHbounds [Code v1.0, accessed 03/03/2022], https://github.com/bradkav/PBHbounds (2022).
[86] E. S. Phinney, A practical theorem on gravitational wave backgrounds, arXiv:astro-ph/0108028.
[87] Xing-Jiang Zhu, E. Howell, T. Regimbau, D. Blair, and Zong-Hong Zhu, Stochastic gravitational wave background from coalescing binary black holes, Astrophys. J. **739**, 86 (2011).
[88] R. A. Allsman *et al.* (MACHO Collaboration), MACHO project limits on black hole dark matter in the 1-30$M_\odot$ solar mass range, Astrophys. J. Lett. **550**, L169 (2001).
[89] P. Tisserand *et al.* (EROS-2 Collaboration), Limits on the macho content of the galactic halo from the EROS-2 survey of the magellanic clouds, Astron. Astrophys. **469**, 387 (2007).
[90] Hiroko Niikura *et al.*, Microlensing constraints on primordial black holes with Subaru/HSC Andromeda observations, Nat. Astron. **3**, 524 (2019).
[91] Hiroko Niikura, Masahiro Takada, Shuichiro Yokoyama, Takahiro Sumi, and Shogo Masaki, Constraints on Earth-mass primordial black holes from OGLE 5-year microlensing events, Phys. Rev. D **99**, 083503 (2019).
[92] Bernard Carr, Martti Raidal, Tommi Tenkanen, Ville Vaskonen, and Hardi Veermäe, Primordial black hole constraints for extended mass functions, Phys. Rev. D **96**, 023514 (2017).
[93] Alexander H. Nitz and Yi-Fan Wang, Search for Gravitational Waves from High-Mass-Ratio Compact-Binary Mergers of Stellar Mass and Subsolar Mass Black Holes, Phys. Rev. Lett. **126**, 021103 (2021).
[94] Alexander H. Nitz and Yi-Fan Wang, Search for Gravitational Waves from the Coalescence of Subsolar-Mass Binaries in the First Half of Advanced LIGO and Virgo's Third Observing Run, Phys. Rev. Lett. **127**, 151101 (2021).
[95] Susanna Barsanti, Valerio De Luca, Andrea Maselli, and Paolo Pani, Detecting Subsolar-Mass Primordial Black Holes in Extreme Mass-Ratio Inspirals with LISA and Einstein Telescope, Phys. Rev. Lett. **128**, 111104 (2022).
[96] Frank C. van den Bosch, Go Ogiya, Oliver Hahn, and Andreas Burkert, Disruption of dark matter substructure: Fact or fiction?, Mon. Not. R. Astron. Soc. **474**, 3043 (2017).
[97] Julian Adamek, Christian T. Byrnes, Mateja Gosenca, and Shaun Hotchkiss, WIMPs and stellar-mass primordial black holes are incompatible, Phys. Rev. D **100**, 023506 (2019).
[98] Laleh Sadeghian, Francesc Ferrer, and Clifford M. Will, Dark matter distributions around massive black holes: A general relativistic analysis, Phys. Rev. D **88**, 063522 (2013).
[99] Francesc Ferrer, Augusto Medeiros da Rosa, and Clifford M. Will, Dark matter spikes in the vicinity of Kerr black holes, Phys. Rev. D **96**, 083014 (2017).

[100] Antony Lewis, Anthony Challinor, and Anthony Lasenby, Efficient computation of CMB anisotropies in closed FRW models, Astrophys. J. **538**, 473 (2000).
[101] Cullan Howlett, Antony Lewis, Alex Hall, and Anthony Challinor, CMB power spectrum parameter degeneracies in the era of precision cosmology, J. Cosmol. Astropart. Phys. 04 (2012) 027.
[102] N. Aghanim *et al.* (Planck Collaboration), Planck 2018 results. VI. Cosmological parameters, Astron. Astrophys. **641**, A6 (2020); **652**, C4(E) (2021).
[103] Massimo Ricotti, Jeremiah P. Ostriker, and Katherine J. Mack, Effect of primordial black holes on the cosmic microwave background and cosmological parameter estimates, Astrophys. J. **680**, 829 (2008).
[104] S. Chandrasekhar, Dynamical friction. I. General considerations: The coefficient of dynamical friction, Astrophys. J. **97**, 255 (1943).
[105] S. Chandrasekhar, Dynamical friction. II. The rate of escape of stars from clusters and the evidence for the operation of dynamical friction, Astrophys. J. **97**, 263 (1943).
[106] S. Chandrasekhar, Dynamical friction. III. A more exact theory of the rate of escape of stars from clusters, Astrophys. J. **98**, 54 (1943).
[107] J. Binney and S. Tremaine, *Galactic Dynamics: Second Edition* (Princeton University Press, Princeton, 2008).
[108] Bradley J. Kavanagh, HaloFeedback [Code, v0.9], https://github.com/bradkav/HaloFeedback (2020).
[109] http://www.et-gw.eu/index.php/etsensitivities.
[110] Matthew Evans, Jan Harms, and Salvatore Vitale, Exploring the sensitivity of next generation gravitational wave detectors, https://dcc.ligo.org/LIGO-P1600143/public (2016).
[111] John Skilling, Nested sampling, AIP Conf. Proc. **735**, 395 (2004).
[112] Edward Higson, Will Handley, Mike Hobson, and Anthony Lasenby, Dynamic nested sampling: An improved algorithm for parameter estimation and evidence calculation, Stat. Comput. **29**, 891 (2019).
[113] Joshua S. Speagle, DYNESTY: A dynamic nested sampling package for estimating Bayesian posteriors and evidences, Mon. Not. R. Astron. Soc. **493**, 3132 (2020).
[114] H. Jeffreys, *The Theory of Probability*, Oxford Classic Texts in the Physical Sciences (Oxford University Press, Oxford, 1998).
[115] Robert E. Kass and Adrian E. Raftery, Bayes factors, J. Am. Stat. Assoc. **90**, 773 (1995).
[116] Curt Cutler *et al.*, What we can learn from multiband observations of black hole binaries, arXiv:1903.04069.
[117] J. Aasi *et al.*, First all-sky search for continuous gravitational waves from unknown sources in binary systems, Phys. Rev. D **90**, 062010 (2014).
[118] Huai-Ke Guo and Andrew Miller, Searching for mini extreme mass ratio inspirals with gravitational-wave detectors, arXiv:2205.10359.
[119] M. J. Graham *et al.*, Candidate Electromagnetic Counterpart to the Binary Black Hole Merger Gravitational-Wave Event S190521g, Phys. Rev. Lett. **124**, 251102 (2020).
[120] Daniel Baumann, Horng Sheng Chia, and Rafael A. Porto, Probing ultralight bosons with binary black holes, Phys. Rev. D **99**, 044001 (2019).
[121] Daniel Baumann, Gianfranco Bertone, John Stout, and Giovanni Maria Tomaselli, Ionization of gravitational atoms, Phys. Rev. D **105**, 115036 (2022).
[122] Daniel Baumann, Gianfranco Bertone, John Stout, and Giovanni Maria Tomaselli, Sharp Signals of Boson Clouds in Black Hole Binary Inspirals, Phys. Rev. Lett. **128**, 221102 (2022).
[123] Martti Raidal, Ville Vaskonen, and Hardi Veermäe, Gravitational waves from primordial black hole mergers, J. Cosmol. Astropart. Phys. 07 (2017) 037.
[124] David F. Chernoff and Lee Samuel Finn, Gravitational radiation, inspiraling binaries, and cosmology, Astrophys. J. Lett. **411**, L5 (1993).
[125] P. Ajith *et al.*, A template bank for gravitational waveforms from coalescing binary black holes. I. Non-spinning binaries, Phys. Rev. D **77**, 104017 (2008); **79**, 129901(E) (2009).
[126] Adam Coogan, PYDD [Code], https://github.com/adamcoogan/pydd (2021).